**RESEARCH PAPER**

# Enhanced Klotho availability protects against cardiac dysfunction induced by uraemic cardiomyopathy by regulating Ca$^{2+}$ handling

José Alberto Navarro-García[1] 🟢 | Angélica Rueda[2] | Tatiana Romero-García[2] | Jennifer Aceves-Ripoll[1] | Elena Rodríguez-Sánchez[1] 🟢 | Laura González-Lafuente[1] | Carlos Zaragoza[3] | María Fernández-Velasco[4] | Makoto Kuro-o[5] | Luis M. Ruilope[1,6,7] | Gema Ruiz-Hurtado[1,6] 🟢

[1]Cardiorenal Translational Laboratory, Institute of Research i+12, Hospital Universitario 12 de Octubre, Madrid, Spain

[2]Departamento de Bioquímica, Centro de Investigación y de Estudios Avanzados del IPN, México City, DF, Mexico

[3]Department of Cardiology, Unidad de Investigación Mixta Universidad Francisco de Vitoria/Hospital Ramon y Cajal (IRYCIS), Madrid, Spain

[4]IdiPAZ Institute for Health Research/CIBER-CV, Madrid, Spain

[5]Division of Anti-ageing Medicine, Centre for Molecular Medicine, Jichi Medical University, Shimotsuke, Tochigi, Japan

[6]CIBER-CV, Hospital Universitario 12 de Octubre, Madrid, Spain

[7]School of Doctoral Studies and Research, European University of Madrid, Madrid, Spain

**Correspondence**
Gema Ruiz-Hurtado, Centro de Investigación, Instituto de Investigación imas12, Hospital Universitario 12 de Octubre, Avenida de Córdoba s/n, 28041, Madrid, Spain.
Email: gemaruiz@h12o.es

**Background and Purpose:** Klotho is a membrane-bound or soluble protein, originally identified as an age-suppressing factor and regulator of mineral metabolism. Klotho deficiency is associated with the development of renal disease, but its role in cardiac function in the context of uraemic cardiomyopathy is unknown.

**Experimental Approach:** We explored the effects of Klotho on cardiac Ca$^{2+}$ cycling. We analysed Ca$^{2+}$ handling in adult cardiomyocytes from Klotho-deficient (*kl/kl*) mice and from a murine model of 5/6 nephrectomy (Nfx). We also studied the effect of exogenous Klotho supplementation, by chronic recombinant Klotho treatment, or endogenous Klotho overexpression, using transgenic mice overexpressing Klotho (*Tg-Kl*), on uraemic cardiomyopathy. Hearts from Nfx mice were used to study Ca$^{2+}$ sensitivity of ryanodine receptors and their phosphorylation state.

**Key Results:** Cardiomyocytes from *kl/kl* mice showed decreased amplitude of intracellular Ca$^{2+}$ transients and cellular shortening together with an increase in pro-arrhythmic Ca$^{2+}$ events compared with cells from wild-type mice. Cardiomyocytes from Nfx mice exhibited the same impairment in Ca$^{2+}$ cycling as *kl/kl* mice. Changes in Nfx cardiomyocytes were explained by higher sensitivity of ryanodine receptors to Ca$^{2+}$ and their increased phosphorylation at the calmodulin kinase type II and protein kinase A sites. Ca$^{2+}$ mishandling in Nfx-treated mice was fully prevented by chronic recombinant Klotho administration or transgenic Klotho overexpression.

**Conclusions and Implications:** Klotho emerges as an attractive therapeutic tool to improve cardiac Ca$^{2+}$ mishandling observed in uraemic cardiomyopathy. Strategies that improve Klotho availability are good candidates to protect the heart from functional cardiac alterations in renal disease.

**KEYWORDS**

Ca$^{2+}$ mishandling, chronic kidney disease, Klotho, ryanodine receptors, uraemic cardiomyopathy

# 1 | INTRODUCTION

The risk of cardiovascular disease increases as renal function declines (Go, Chertow, Fan, McCulloch, & Hsu, 2004; Herzog et al., 2011), and cardiovascular disease is the major cause of mortality in patients with chronic kidney disease (CKD). Among the components of bone mineral metabolism, alterations in Klotho protein and the **fibroblast growth factor (FGF)-23** axis seem to be important contributors to the high cardiovascular risk in this patient group (Gutiérrez et al., 2008; Isakova et al., 2011; Isakova et al., 2018). FGF-23 is a circulatory hormone that mainly targets the kidney, where it controls systemic phosphate homeostasis. The phosphaturic action of FGF-23 is dependent on renal expression of membrane-bound Klotho, a powerful regulator of aging and lifespan (Kuro-o et al., 1997). Klotho is predominantly synthesised in the kidney where it binds to FGF receptors (FGFRs), increasing their affinity for FGF-23 and promoting urinary phosphate excretion (Urakawa et al., 2006). Klotho expression diminishes as renal function deteriorates, and this reduction might be responsible for the resistance to FGF-23 observed in the course of CKD (Pavik et al., 2013). Membrane-bound Klotho can be shed by the action of secretases and released into circulation as a soluble form. Circulating soluble Klotho (sKL) has several functions that are poorly understood, including an apparently cardioprotective action that is independent of FGF-23 and phosphate (Hu et al., 2017; Xie et al., 2012; Xie, Yoon, An, Kuro-o, & Huang, 2015). Accordingly, high levels of sKL are associated with a lower risk of developing cardiovascular disease, and low-sKL levels are related to cardiac dysfunction, at least when advanced age is considered (Semba et al., 2011). Several recent clinical studies have shown that low circulating sKL levels are associated with an elevated risk of cardiovascular mortality or hospitalisation due to cardiovascular events (including heart failure development, myocardial infarction, or stroke) in patients with stable ischaemic heart disease (Bergmark et al., 2019) or on haemodialysis (Memmos et al., 2019). Thus, there is a need to determine whether Klotho can directly regulate cardiomyocyte function and cardiac rhythm in the setting of renal disease and to elucidate the underlying mechanisms involved in the potential cardioprotective actions of Klotho.

The increased cardiovascular morbidity and mortality linked to renal dysfunction are due, at least in part, to the high prevalence of heart failure and arrhythmias in patients with CKD, mainly those undergoing dialysis (Charytan et al., 2016; Verde et al., 2016; Wanner, Amann, & Shoji, 2016). Indeed, cardiovascular deaths account for $\sim$50% of all deaths in CKD, especially in patients on dialysis, which is chiefly due to fatal arrhythmias (Coll et al., 2018). Alterations in intracellular $Ca^{2+}$ cycling, such as changes in $Ca^{2+}$ release from the sarcoplasmic reticulum (SR) mediated by **ryanodine receptor (RyR)** channels in cardiomyocytes, are well-documented mechanisms involved in cardiac dysfunction and arrhythmias (Bers, 2014; Nattel, Maguy, Le Bouter, & Yeh, 2007). Cardiac muscle contraction is triggered by an action potential that induces a small $Ca^{2+}$ influx via sarcolemmal L-type $Ca^{2+}$ ($I_{CaL}$) channels, triggering a greater release of $Ca^{2+}$

**What is already known**

- CKD patients present alterations in mineral metabolism components including a decline in Klotho protein expression.
- Recent studies point to Klotho as a new anti-aging factor with cardioprotective properties.

**What this study adds**

- Klotho deficiency alters systolic $Ca^{2+}$ release and contractile function and increases pro-arrhythmogenic diastolic $Ca^{2+}$ leak.
- Recombinant Klotho treatment prevents cardiac $Ca^{2+}$ mishandling and RyR hypersensitivity in CKD.

**What is the clinical significance**

- Recombinant Klotho is a promising new prophylactic strategy to reduce cardiac functional alterations in CKD.

from the SR by RyR channels. This elevation in cardiomyocyte $Ca^{2+}$ transients stimulates cardiomyocyte contraction (Bers, 2002). Relaxation is initiated when $Ca^{2+}$ is pumped out from the cytosol by two chief mechanisms: (i) $Ca^{2+}$ re-uptake to the SR by the $Ca^{2+}$-ATPase 2a pump **(SERCA2a)** ($\sim$92%) and (ii) $Ca^{2+}$ extrusion to the extracellular medium by the $Na^+/Ca^{2+}$ exchanger **(NCX)** ($\sim$7%) (Bers, 2002). An increase in RyR channel sensitivity, evoking higher spontaneous diastolic SR-$Ca^{2+}$ leak, is known to increase the risk of malignant arrhythmias. Whether $Ca^{2+}$ handling alterations also occur in the context of CKD and whether Klotho could induce cardioprotection in this context by modulating intracellular $Ca^{2+}$ handling remain unknown.

Here, we used Klotho-deficient (*kl/kl*) mice to determine whether Klotho is necessary for correct cardiomyocyte function. Furthermore, we established a murine model of CKD by 5/6 nephrectomy to test the hypothesis that strategies directed to improve Klotho availability—supplied exogenously (recombinant) or endogenously (by enhancing its expression)—could prevent cardiac dysfunction related to intracellular $Ca^{2+}$ mishandling in uraemic cardiomyopathy.

# 2 | METHODS

## 2.1 | Animals

All animal care and experimental procedures complied with the guidelines for ethical NIH Guide for the Care and Use of Laboratory Animals and Guidelines for Ethical Care and Welfare (2013/175) of Experimental Animals of the European Union (2010/63/EU) and were

approved by the Bioethical Committee of the Universidad Autónoma de Madrid, and by the General Direction of Agriculture and the Environment at the Environment Council of Madrid (PROEX 053/16). Animal studies are reported in compliance with the ARRIVE guidelines (Percie du Sert et al., 2020) and with the recommendations made by the British Journal of Pharmacology (Lilley et al., 2020).

Male C57BL/6 J mice (20–23 g, 6 weeks of age; IMSR_JAX:000664) were purchased from Charles River Laboratories International Inc. (Wilmington, MA, USA; SCR_003792). Mice were bred and housed under specific pathogen-free conditions in the Experimental Animal Centre of Hospital Universitario 12 de Octubre, Madrid, Spain. Animals were maintained at controlled temperature (23–25 °C) on a 12-hr light/dark cycle with *ad libitum* access to water and a standard diet (ROD14, Altromin Spezialfutter GmbH & Co. KG, Lage, Germany). Animals were housed in groups of four per cage of 553 cm$^2$ by 20.8-cm depth (polysulfone cage type II L, SODISPAN, Madrid, Spain) with standard wood chip (ECO-PURE 7 Chips, Tapvei®, Estonia). All efforts were made to reduce the number of animals required to obtain reliable results and minimise the suffering of the animals based on the 3Rs rule of replacement, refinement, and reduction. The viability of the ventricular cardiomyocyte isolation process was established when the percentage of relaxed and rod-shaped cardiomyocytes in total cell count was equal or greater than 70% (Shioya, 2007). No difference was observed in the viability of the cardiomyocyte isolation process between all experimental groups.

## 2.2 | Experimental model of chronic kidney disease and treatments

Mice underwent Sham or 5/6 nephrectomy (Nfx) surgery to induce CKD. Nfx was performed in a two-step procedure under isoflurane anaesthesia (1.5% v/v, isoflurane/oxygen). In the first step, an abdominal incision was made, and the upper and lower poles of the left kidney were removed, leaving an intact segment around the hilum (experimental week 0). One week later, a dorsal incision was made, and the right kidney was completely removed (Gagnon & Gallimore, 1988). Sham-operated mice followed the same protocol without the removal of the kidneys. Meloxicam (0.06 ml·kg$^{-1}$, s.c. single dose) was used as analgaesia after surgeries. After that, Sham or Nfx surgery mice were blindly randomised to receive either vehicle solution (0.9% sodium chloride) or murine recombinant Klotho (rKL, 0.01 mg·kg$^{-1}$ per day). Mice were treated at the same hour in the morning every day for 6 weeks by i.p. injection as described before (Hu et al., 2017). Macroscopic parameters were analysed in 16 Sham, 20 Nfx, 17 Sham+rKL and 22 Nfx+rKL mice. Ten mice in each group were used for biochemical parameters, five to seven mouse hearts per group were used for ryanodine binding analysis, and five mice per group were used for echocardiogram analysis. Cardiomyocytes obtained from five Sham, six Nfx, five Sham+rKL, and six Nfx+rKL mice were used for Ca$^{2+}$ handling analysis.

## 2.3 | Echocardiography

Mouse hearts were visualised by echocardiography, using the Vivid Q ultrasound system (GE Healthcare), with a coupled linear sonar of 14 MHz. A single investigator, blinded to the experimental groups, performed the analysis. Measurements were carried out with mice under isoflurane anaesthesia (1.5% v/v, isoflurane/oxygen) in order to keep a heart rate of about 400 beats min$^{-1}$. Body hair was shaved, and parasternal images of the short axis of the heart were obtained in a bidimensional mode (B), for anatomical visualisation. Taking as a reference the papillary muscles, we carried out the functional analysis of cardiac contractility by an ultrasound M mode, to determine ejection fraction (EF) using cardiac analysis software.

## 2.4 | Klotho-hypomorphic and Klotho-overexpressing mice

Transgenic (*Tg-Kl*) and Klotho-hypomorphic (*kl/kl*) mice were kindly provided by Dr. Kuro-o and bred in our animal facilities.

Male *kl/kl* mice (8 g of weight) and their +/+ littermates (20 g of weight) were used at 6–8 weeks of age. Macroscopic parameters were analysed in 22 +/+ and 19 *kl/kl* mice. Ten mice in each group were used for biochemical parameter analysis, and five mice per group were used for Ca$^{2+}$ handling analysis.

*Tg-Kl* 6-week-old mice with a weight between 20 and 22 g underwent Sham (Sham-*Tg-Kl*) or Nfx (Nfx-*Tg-Kl*) surgery as described before. Biochemical parameters were analysed in five Sham-*Tg-Kl* and seven Nfx-*Tg-Kl* mice, and five Sham-*Tg-Kl* mice and Nfx-*Tg-Kl* six mice were used for Ca$^{2+}$ handling analysis.

## 2.5 | Serum and urine biochemistry

Plasma levels of phosphorus (Abcam, Cambridge, UK), urea and blood urea nitrogen (BUN) (BioAssays System, Hayword, CA), and FGF-23 (Immunotopics, Inc., San Clemente, CA) were measured by ELISA following the manufacturers' instructions. Mouse soluble α-Klotho assay kit (IBL International, Hamburg, Germany) was used to measure sKL in urine samples.

## 2.6 | Cardiomyocyte isolation

Adult male mice (6–8-week-old +/+ or *kl/kl*, 14-week-old WT-Sham, Nfx, Sham+rKL or Nfx+rKL, and *Tg-Kl*-Sham or *Tg-Kl*-Nfx, blindly selected) were anaesthetised with sodium pentobarbital-heparin (100 mg/kg, i.p.). Mice were sacrificed, and hearts were rapidly removed and cannulated via the ascending aorta on a Langendorff perfusion system (Navarro-García et al., 2019; Ruiz-Hurtado et al., 2015). Hearts were retrogradely perfused with calcium-free Tyrode's solution supplemented with EGTA (0.2 mmol·L$^{-1}$) for 3 min followed by Tyrode's solution containing 0.1 mmol·L$^{-1}$ of CaCl$_2$, 1 mg·mL$^{-1}$ of type

II collagenase (Worthington, Lakewood, NY), and 1 mg·mL$^{-1}$ of BSA for 3–4 min at room temperature. Digested hearts were filtered through a nylon mesh (250 μm) and centrifuged at 280 x $g$ for 3 min at room temperature. The pellet was re-suspended in Tyrode's solution containing 0.5 mmol·L$^{-1}$ of CaCl$_2$ and centrifuged again. Finally, the pellet was re-suspended in Tyrode's solution containing CaCl$_2$ (1 mmol·L$^{-1}$). Tyrode's solution contained (in mmol·L$^{-1}$): 130 NaCl, 5.4 KCl, 0.4 NaH$_2$PO$_4$, 0.5 MgCl$_2$, 25 HEPES, and 22 glucose. The pH was adjusted to 7.4 with LiOH.

## 2.7 | Confocal Ca$^{2+}$ image analysis

Isolated ventricular cardiomyocytes were loaded with the membrane-permeant fluorescent Ca$^{2+}$ indicator Fluo-3 AM (5 μmol·L$^{-1}$; Invitrogen, Carlsbad, CA) for 30 min at room temperature. Line-scan Ca$^{2+}$ images were obtained using confocal microscopy (Meta Zeiss LSM 510, objective w.i. 40×, n.a. 1.2) at the speed of 1.5 ms/line (1,000 lines per image) with a pixel size of 0.07 μm for recording Ca$^{2+}$ transients, Ca$^{2+}$ sparks, and Ca$^{2+}$ wave images, while for caffeine and arrhythmia protocols, confocal images were obtained at a speed of 3 ms/line (10,000 lines per image) for a total duration of 30 s. All Ca$^{2+}$ images were corrected for the background fluorescence. In a set of experiments, Fluo-3-loaded cells were placed in a field stimulation chamber with two parallel platinum electrodes and filled with Tyrode's solution. Cells were allowed to settle at the bottom of the chamber and paced at 2 Hz with a pulse generator (CS-420, Cibertec) during 1–2 min to allow steady-state intracellular Ca$^{2+}$ transients. Then, a line was selected always in parallel to the longitudinal cell axis to be able to measure the associated cell shortening; and Ca$^{2+}$ imaging recordings were manually initiated with the time-lapse plug-in included in Zen 2009 Imaging Software (12.09, ZEISS).

The amplitude of Ca$^{2+}$ transients was calculated by averaging the fluorescence values in a 1.4-μm frame over time. The amplitude of Ca$^{2+}$ transients was estimated as $F/F_0$, where $F$ was the maximum value of fluorescence signal during electrical stimulation and $F_0$ was the basal fluorescence at rest at each position determined as the average of the 50 lowest values on the fluorescence transient. Moreover, $\Delta F/F_0$ was calculated using the following formula $\Delta F/F_0 = (F - F_0)/F_0$. SERCA2a function was indirectly estimated by the decay time constant of intracellular Ca$^{2+}$ transients, termed $Tau$, which was obtained by fitting the descending phase of the fluorescence trace to a single exponential. $K$ SERCA2a refers to the SR-dependent fraction of the rate constant of decay of the systolic Ca$^{2+}$ transient and was measured by subtracting the rate constant of decay of the caffeine-evoked transients from that of the systolic Ca$^{2+}$ transients (Bode et al., 2011). Cell shortening was measured as the difference of cardiomyocytes length between electrical stimulation and resting. Cell shortening was expressed as the percentage of cell's shortening length. Cell shortening profiles were obtained offline by measuring the cell length from each line of Ca$^{2+}$ transient images. SR Ca$^{2+}$ load was estimated by perfusing cardiomyocytes with 10 mmol·L$^{-1}$ of caffeine immediately after field stimulation.

Caffeine depletes the SR of Ca$^{2+}$ stores. Caffeine-evoked Ca$^{2+}$ transients' amplitude was measured as peak $F/F_0$ and was used to rate the global SR Ca$^{2+}$ load.

In a set of experiments, spontaneous Ca$^{2+}$ sparks were recorded in quiescent Fluo-3-loaded cardiomyocytes when electrical stimulation was stopped. Ca$^{2+}$ sparks were considered as brief, located, and rapid increments in Ca$^{2+}$ fluorescence. Ca$^{2+}$ spark regions are determined as the sites where fluorescence signal increased by at least four times the standard deviation of the image fluorescence. These inclusion criteria limited false events while detecting most sparks (Cheng et al., 1999). Spontaneous Ca$^{2+}$ transients and Ca$^{2+}$ waves in quiescent cardiomyocytes were detected as substantial spontaneous Ca$^{2+}$ synchronic or non-synchronic release, respectively. The arrhythmic activity was measured as abnormal spontaneous Ca$^{2+}$ transients with automatic contractions in cardiomyocytes during a specific protocol, consisting of three cycles of seven electric pulses followed by a recovery period.

All Ca$^{2+}$ images were processed and analysed offline using IDL (RSI) software and homemade routines.

## 2.8 | Ryanodine binding analysis

[$^3$H]-Ryanodine binding experiments were performed with homogenates of left ventricles from individual hearts, as described earlier (de Alba-Aguayo et al., 2017). Specific binding was defined as the difference between the binding in the absence (total binding) and presence (non-specific binding) of 20 μmol·L$^{-1}$ of unlabelled ryanodine. The incubation medium contained (in mmol·L$^{-1}$) the following: KCl 200, HEPES 20, and EGTA-K salt 1, pH 7.2 with KOH. CaCl$_2$ was added as necessary to establish free Ca$^{2+}$ at 100 nmol·L$^{-1}$ (equivalent to diastolic Ca$^{2+}$ concentration) and 10 μmol·L$^{-1}$ (equivalent to systolic Ca$^{2+}$ concentration). Ca$^{2+}$-EGTA ratios were calculated using the WEBMAXCLITE program v1.15 (https://web.stanford.edu/~cpatton/webmaxc/webmaxclite115.htm). Data analysis was performed using Origin (v8.1; OriginLab Corporation, Northampton, MA, USA).

## 2.9 | Western blotting

Immunoblotting analysis complies with the recommendations on immunoblotting and immunohistochemistry in pharmacology (Alexander et al., 2018). Hearts were homogenised in 400 μl of homogenisation buffer (0.05 mol·L$^{-1}$ of Tris, 0.32 mol·L$^{-1}$ of sucrose, 0.5% CHAPS, 0.5 μmol·L$^{-1}$ of okadaic acid, and the protease inhibitors PMSF (0.1 mmol·L$^{-1}$), leupeptin (12 μmol·L$^{-1}$), aprotinin (0.2 μmol·L$^{-1}$) and benzamidine (0.5 mmol·L$^{-1}$), and the pH was adjusted to 7.0. Homogenates were centrifuged at 2800 x$g$ for 10 min at 4 °C. Supernatants were collected in microtubes, and 20 μg of total protein was used for western blotting. Samples were re-suspended in SDS-PAGE loading buffer (4× Laemmli Sample Buffer; Bio-Rad, Hercules, CA, USA) with 10%

β-mercaptoethanol and were heated for 5 min at 90 °C. Samples were loaded on 4–20% SDS-PAGE gradient gels (Criterion™ TGX™ Precast Gels, Bio-Rad). Proteins were electrophoretically transferred onto PVDF membranes (Trans-Blot® Turbo™ Midi Format, 0.2 μmol·$L^{-1}$ PVDF, Bio-Rad) on a semi-dry transfer system (Trans-Blot SD, Bio-Rad) at 2.5 A, 25 V for 10 min. Membranes were blocked with 5% BSA and TBS-$T_{20}$ buffer (50 mmol·$L^{-1}$ of Tris–HCl, 150 mmol·$L^{-1}$ of NaCl, and 0.1% Tween-20). Fresh antibodies solutions were used for immunoblotting. Antibodies used were as follows: rabbit polyclonal IgG anti-phosphoRyR $Ser^{2814}$ (AB_2617055) at 1:2,000 dilution and rabbit polyclonal IgG anti-phosphoRyR $Ser^{2030}$ at 1:2,000 dilution (A010-31 and A010-32, respectively, both from Badrilla, Leeds, UK), mouse monoclonal IgG1 anti-RyR (AB_2183054) at 1:2,500 dilution, and mouse monoclonal IgG1 anti-GAPDH (AB_2536381) at 1:400,000 dilution (MA3-916 and AM4300, respectively, both from Thermo Fisher Scientific, Waltham, MA, USA). HRP-conjugated secondary antibodies used were as follows: anti-mouse IgG kappa (AB_2687626) at 1:5,000 dilution and mouse anti-rabbit (AB_628497) at 1:5,000 dilution (sc-516102 and sc-2357, respectively, both from Santa Cruz Biotechnology, Dallas, TX, USA).

## 2.10 | RNA isolation and quantitative real-time PCR

Total RNA was isolated from mouse hearts using the RNeasy Mini Kit (Qiagen, Hilden, Germany). Quality and quantity of RNA were assessed with NanoDrop One Microvolume UV–Vis Spectrophotometer (Thermo Fischer Scientific, Waltham, MA), and 2 μg of RNA was reverse-transcribed to cDNA using High-Capacity cDNA Reverse Transcription Kit (Applied Biosystems, Foster City, CA). Quantitative RT-PCR was performed using FastStart Essential DNA Green Master (Roche, Basel, Switzerland) in 10-μl total reaction volume on a LightCycler® 480 II (Roche, Basel, Switzerland) at optimised thermocycling settings. Relative gene expression was normalised to the ribosomal housekeeping gene 36b4 (RPLP0) and evaluated using the $2^{-\Delta\Delta Ct}$ method. The primer sequences (5′–3′) for SERCA2a (*Atp2a2*), 36b4, collagen I (*col1a1*), collagen III (*col3a1*), and atrial natriuretic peptide (*Nppa*) were as follows: *Atp2a2-Forward* TAAATGCCCGCTGTTTTGCT; *Atp2a2-Reverse* TTGTCATCTGCCAGG ACCAT; *36b4-Forward* AGATGCAGCAGATCCGCAT; *36b4-Reverse* GTTCTTGCCCATCAGCACC; *col1a1-Forward* AATGGCACGG CTGTCTGCGA; *col1a1-Reverse* AGCACTCGCCCTCCCGTCTT; *col3a1-Forward* CTGTAACATGGAAACTGGGGAAA; *col3a1-Reverse* CCATAGCTGAACTGAAAACCACC; *Nppa-Forward* CTGGGACCCC TCCGATAGAT; and *Nppa-Reverse* CACTCTGGGCTCCAATCCTG.

## 2.11 | Data and statistical analysis

Group size estimation was designed to be equal, yielding 90% power. Inferential statistics were used to summarise the data from ≥5 animals per group. Any inequalities between experimental groups were

exclusively owing to the assumed animal losses related to the specific surgery (5/6 nephrectomy) used in the study. The number of animals used in this study was based on power calculation and was a total of 122. The mouse was considered as the experimental unit for echocardiography, western blotting, and ryanodine binding analyses; and the whole heart was used for measurement and referred to as "N." For all $Ca^{2+}$ handling studies, the cardiomyocyte was considered as the experimental unit and referred to as "n" after assessing the absence of false positives and independence of the obtained data and the absence of clustering estimated by the intra-cluster correlation coefficient (ICC) tests for all cellular data sets and experimental models used. For $Ca^{2+}$ handling studies, both cell number (n) and animal number (N) are shown, and cardiomyocytes were isolated from at least five mice in each experiment. Data are presented as mean ± SEM. The data and statistical analysis comply with the recommendations on experimental design and analysis in pharmacology (Curtis et al., 2018). The data that support the results obtained in this study are available upon reasonable request from the corresponding author. Statistical significance was evaluated using paired Student's test, $\chi^2$ test, or ANOVA with Newman–Keuls multiple-comparison tests when appropriate (only with homogeneity and if *F* was significant). The Kolmogorov–Smirnov test was used to determine the Gaussian distribution of the values. All *P*-values are two-tailed, and *P*-values < 0.05 were considered statistically significant. All analyses were performed using GraphPad Prism v6.0 (GraphPad Software Inc., San Diego, CA; SCR_002798) or Origin Pro v9.0 (OriginLab Corp., Northampton, MA; SCR_014212).

## 2.12 | Materials

EGTA, sodium chloride, potassium chloride, monosodium phosphate, magnesium chloride, HEPES, glucose, lithium hydroxide, potassium hydroxide, leupeptin, aprotinin, benzamidine, β-mercaptoethanol, Tween 20, and caffeine were purchased from Sigma-Aldrich (Milan, Italy). Isoflurane was purchased from Abbie Spain (Madrid, Spain). CHAPS was purchased from GE Healthcare (Chicago, IL, USA). Okadaic acid-K salt was purchased from Santa Cruz Biotechnology (Dallas, TX, USA); 4× Laemmli Sample Buffer and TBS were purchased from Bio-Rad (Hercules, CA, USA). Pentobarbital was purchased from Vetoquinol (Madrid, Spain). Heparin was purchased from ROVI (Madrid, Spain). All the reagents have been dissolved in distilled $H_2O$, when necessary.

## 2.13 | Nomenclature of targets and ligands

Key protein targets and ligands in this article are hyperlinked to corresponding entries in the IUPHAR/BPS Guide to PHARMACOLOGY (http://www.guidetopharmacology.org) and are permanently archived in the Concise Guide to PHARMACOLOGY 2019/20 (Alexander, Fabbro et al., 2019a, b; Alexander, Kelly et al., 2019; Alexander, Mathie et al., 2019).

# 3 | RESULTS

## 3.1 | Klotho deficiency alters intracellular Ca²⁺ handling and cardiomyocyte shortening and increases pro-arrhythmogenic Ca²⁺ events

To examine whether Klotho is needed for a correct cardiac function related to cardiomyocyte $Ca^{2+}$ handling, we used an experimental model of uraemia characterised by deficiency in Klotho, the Klotho-hypomorphic (*kl/kl*) mouse. Macroscopic analysis showed that *kl/kl* mice were significantly smaller than their littermates *+/+* (Figure 1a, Table 1). Similarly, heart and kidney weights were significantly lower in *kl/kl* mice than in *+/+* mice (Table 1). Heart weight to body weight ratio (HW/BW) was significantly higher in *kl/kl* mice than in *+/+* mice (Table 1). However, this increase in HW/BW ratio was not accompanied by signs of cellular hypertrophy in *kl/kl* mice, because cardiomyocyte area was significantly smaller in *kl/kl* mice than in *+/+* mice (1,471 ± 39.7 vs. 2,428 ± 67.7 μm²). We also measured mRNA expression levels of the **atrial natriuretic peptide (ANP**; *Nppa*) by quantitative RT-PCR in hearts from *kl/kl* and *+/+* mice as a classic marker of cellular hypertrophy, finding *Nppa* gene expression not different between groups (1.037 ± 0.13 for *+/+* vs. 0.974 ± 0.07 for *kl/kl*, arbitrary units). Moreover, to assess whether the absence of Klotho expression could be accompanied by myocardial fibrosis development, collagen I and III levels were also analysed through *col1a1* or *col3a1* gene expression levels. The *kl/kl* mice showed reduced levels of collagen I and III, compared with those in *+/+* mice (1.008 ± 0.06 vs. 0.267 ± 0.03 arbitrary units, for *col1a1*; 1.162 ± 0.03 vs. 1.014 ± 0.08, for col3a1). Therefore, the increment in HW/BW ratio in *kl/kl* mice was not due to cardiomyocyte hypertrophy or cardiac fibrosis development. On the other hand, as expected, kidney function was impaired in *kl/kl* mice, as reflected by the significant increase in the levels of urea, BUN, and FGF-23 relative to *+/+* littermates (Table 1). However, no differences in serum levels of phosphate were observed between both groups (Table 1), possibly as consequence of the phosphaturic action induced by the very high FGF-23 levels.

We next analysed intracellular $Ca^{2+}$ handling in cardiomyocytes isolated from both experimental groups. We studied systolic $Ca^{2+}$ release through electrically evoked intracellular $Ca^{2+}$ transients. Figure 1b shows representative line-scan $Ca^{2+}$ images (bottom panels) and fluorescence profiles (upper panels) obtained during electrical field stimulation at 2 Hz, corresponding to *+/+* (left panel) and *kl/kl* (right panel) cardiomyocytes. Similar differences in the amplitude of $Ca^{2+}$ transients ($F/F_0$) were found between *+/+* and *kl/kl* mice analysed by cells or by hearts (3.46 ± 0.11 vs. 1.84 ± 0.05 or 3.46 ± 0.18 vs. 1.84 ± 0 ± 0.08, respectively). Intracellular $Ca^{2+}$ transients amplitude ($F/F_0$) was significantly lower in *kl/kl* cells than in *+/+*
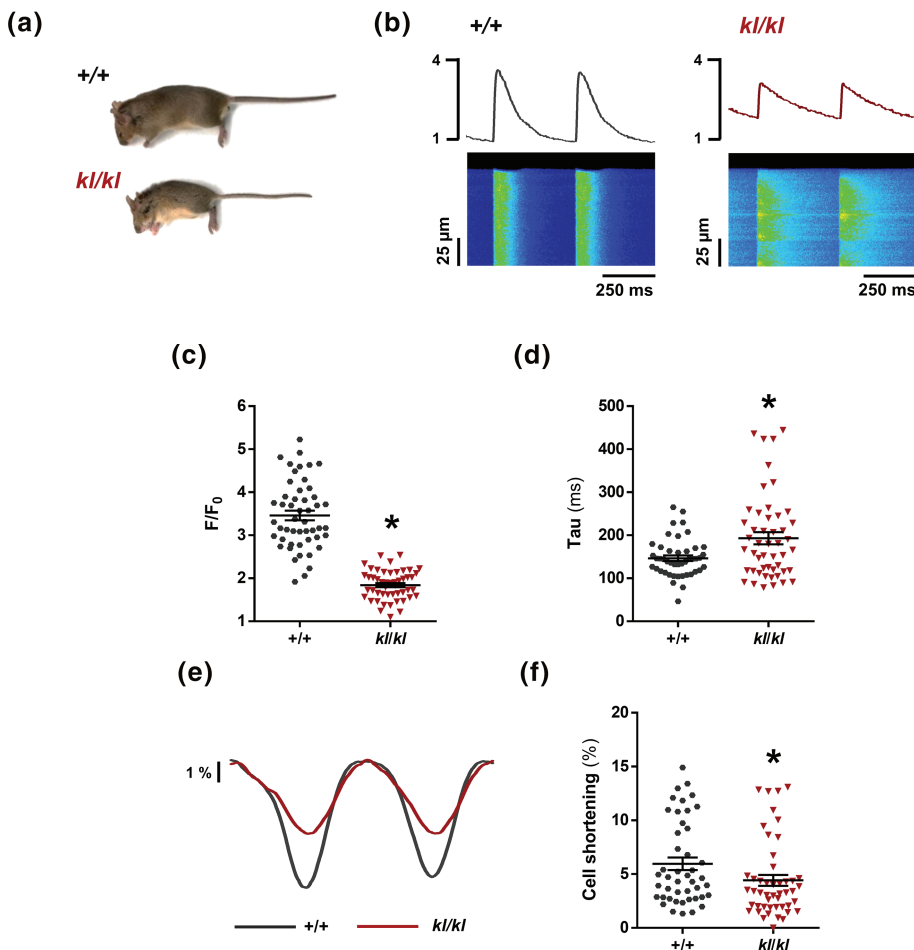


**FIGURE 1** Klotho deficiency impairs systolic $Ca^{2+}$ release and induces contractile dysfunction. (A) Appearance of 7-week-old wild-type (*+/+*) mouse and its Klotho-hypomorphic (*kl/kl*) littermate. (B) Line-scan images and fluorescence profiles of cardiomyocytes under 2-Hz field stimulation. (C and D) Mean values of peak ($F/F_0$) (C) and time of decay (*Tau*) (D) of electrically evoked $Ca^{2+}$ transients in *+/+* (n = 50 cells/N = 5 mice) and *kl/kl* samples(n = 49 cells/N = 5 mice). (E) Cell shortening profiles of cardiomyocytes. (F) Percentage of cell contraction of *+/+* (n = 50 cells/N = 5 mice) and *kl/kl* (n = 49 cells/N = 5 mice). Data are shown as mean ± SEM. *P < 0.05, significantly different from *+/+* mice

**TABLE 1**  Macroscopic and biochemical parameters in Klotho-hypomorphic mice

|  | +/+ | kl/kl |
|---|---|---|
| *Macroscopic parameters* |  |  |
| Body weight (BW, g) | 23.7 ± 0.3 (N = 22) | 8.4 ± 0.3* (N = 19) |
| Heart weight (HW, mg) | 169.0 ± 6.2 (N = 22) | 102.7 ± 5.3* (N = 19) |
| HW/BW ratio | 7.10 ± 0.20 (N = 22) | 12.37 ± 0.67* (N = 19) |
| Kidney weight (KW, mg) | 155.9 ± 4.4 (N = 22) | 58.1 ± 2.3* (N = 19) |
| *Biochemical parameters* |  |  |
| Urea (mg·L$^{-1}$) | 357 ± 25 (N = 10) | 646 ± 49* (N = 10) |
| BUN (mg·L$^{-1}$) | 167 ± 12 (N = 10) | 302 ± 23* (N = 10) |
| Phosphorus (mg·L$^{-1}$) | 133. ± 7 (N = 10) | 1215 ± 8 (N = 10) |
| FGF-23 (pg·ml$^{-1}$) | 268.3 ± 36.7 (N = 10) | 457,318 ± 57,566* (N = 10) |

*Note.* Data for macroscopic and biochemical parameters per experimental group are reported as mean ± SEM. BUN, blood urea nitrogen; BW, body weight; FGF-23, fibroblast growth factor 23; HW, heart weight; KW, kidney weight.
*$P < 0.05$, significantly different from +/+ mice.

cells (Figure 1c). In addition, cardiomyocytes from *kl/kl* mice showed a decrease in $\Delta F/F_0$, indicating a significant decrease in the global intracellular $Ca^{2+}$ transient in *kl/kl* cells (Figure S1). The time constant of $Ca^{2+}$ transients decay, *Tau*, was significantly longer in *kl/kl* cells than in +/+ cells (Figure 1d). This is also illustrated in the representative fluorescence profiles normalised by the peak of $Ca^{2+}$ transients from +/+ and *kl/kl* cells (Figure S2), indicating that the SERCA2a pump was working less efficiently in *kl/kl* cardiomyocytes. Because this slower time decay of $Ca^{2+}$ transients could indicate a worse SR-$Ca^{2+}$ re-uptake by SERCA2a, we analysed the cardiac mRNA levels of SERCA2a in hearts from +/+ and *kl/kl* mice. As shown in Figure S3, SERCA2a expression was significantly reduced in the hearts of *kl/kl* mice compared with +/+ mice. Moreover, *K* SERCA2a, the SR-dependent contribution of the rate constant of decay of the systolic $Ca^{2+}$ transient, was also determined by subtracting the rate constant of decay of the caffeine-evoked transients from that of the systolic $Ca^{2+}$ transients. *K* SERCA2a was significantly lower in *kl/kl* mice than in +/+ mice (Figure S4), supporting a diminished SERCA2a-mediated $Ca^{2+}$ re-uptake. We next addressed whether the decrease in systolic $Ca^{2+}$ release impaired contractile function. Representative cell shortening profiles of cardiomyocytes are shown in Figure 1e. Cell shortening was significantly lower in *kl/kl* cells than in +/+ cells (Figure 1f). Changes in systolic $Ca^{2+}$ release can be related to alterations in SR-$Ca^{2+}$ load. To study this, we applied caffeine to isolated Fluo-3-loaded cardiomyocytes to empty the SR of $Ca^{2+}$. Representative line-scan images of caffeine-evoked $Ca^{2+}$ transients are shown in Figure 2a. Results showed that the amplitude ($F/F_0$) of caffeine-evoked $Ca^{2+}$ transients was significantly lower in *kl/kl* cardiomyocytes than in cells from their littermates (Figure 2b). Caffeine-evoked $Ca^{2+}$ transient decay in cardiomyocytes from *kl/kl* mice was not different from that in +/+ mice, suggesting no alterations in $Ca^{2+}$ extrusion through the NCX (Figure S5).

We next analysed whether the change in SR-$Ca^{2+}$ load was related to alterations in diastolic $Ca^{2+}$ leak. Representative line-scan images of $Ca^{2+}$ spark recordings are shown in Figure 2c. We observed a significantly higher frequency of $Ca^{2+}$ sparks in *kl/kl* cardiomyocytes

than in +/+ cells (Figure 2d). Spontaneous calcium release (SCR) was also studied during diastolic recordings; spontaneous intracellular $Ca^{2+}$ transients and $Ca^{2+}$ waves were considered forms of SCR (Figure 2e, left and right panels, respectively). *kl/kl* cardiomyocytes had a significantly higher prevalence of SCR than +/+ cells (Figure 2f). Finally, we measured pro-arrhythmogenic $Ca^{2+}$ events in cardiomyocytes isolated from both groups of mice. Figure 2g shows representative line-scan images of the pacing protocol. Pro-arrhythmogenic $Ca^{2+}$ release was significantly higher in *kl/kl* cardiomyocytes than in +/+ cells (Figure 2h).

## 3.2 | Chronic recombinant Klotho administration prevents the cardiac dysfunction and impaired systolic $Ca^{2+}$ release induced by experimental chronic kidney disease

We next employed a classical model of CKD (5/6 nephrectomy) to conduct a detailed analysis of the functional cardiac consequences in a uraemic context. Moreover, based on previous evidence demonstrating the cardioprotective action of exogenous Klotho supplementation (Hu et al., 2017; Nowak et al., 2014) and after confirming that Nfx mice have significantly decreased Klotho levels compared with Sham mice (Figure S6), we analysed the effect of recombinant Klotho (rKL) administration on cardiac function and $Ca^{2+}$ cycling. The experimental design is shown in Figure 3a. Macroscopic analysis revealed that Nfx-induced overall body weight loss independently of subsequent treatment (Table 2). Kidney weight was also significantly lower in Nfx mice than in Sham mice, both in vehicle-treated and rKL-treated mice. No differences were observed in heart weight or HW/BW ratio among groups (Table 2). No evidence of cellular hypertrophy was observed in CKD mice as demonstrated by similar cardiomyocyte area (3,192 ± 93.2 vs. 3,187 ± 92.7) and ANP expression levels (1.170 ± 0.51 vs. 0.300 ± 0.05) between Sham and Nfx mice. To assess whether uremic cardiomyopathy induces myocardial fibrosis development, collagen I and III levels were analysed through
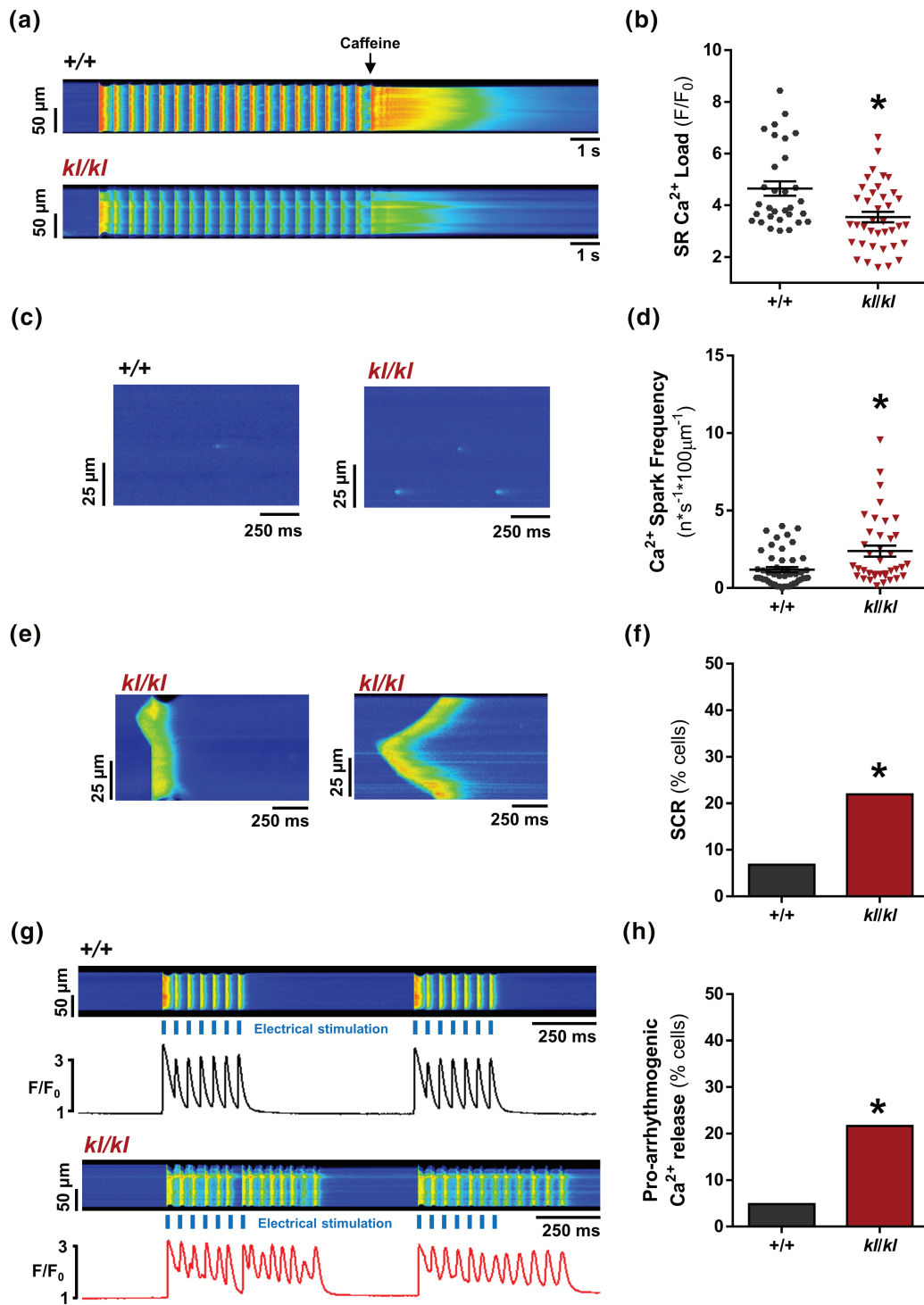
**FIGURE 2** Klotho deficiency reduces SR-Ca$^{2+}$ load and increases diastolic Ca$^{2+}$ leak and pro-arrhythmogenic events. (A) Line-scan images of cardiomyocytes under 2-Hz field stimulation perfused with caffeine. (B) Mean values of caffeine-evoked Ca$^{2+}$ transients amplitude expressed as peak ($F/F_0$) in +/+ ($n = 31$ cells/$N = 5$ mice) and kl/kl ($n = 39$ cells/$N = 5$ mice). (C) Line-scan images of spark recordings in quiescent cardiomyocytes. (D) Mean values of Ca$^{2+}$ spark frequency in +/+ (664 sparks, $n = 48$ cells/$N = 5$ mice) and kl/kl (630 sparks, $n = 39$ cells/$N = 5$ mice). (E) Line-scan images of spontaneous Ca$^{2+}$ release (SCR) as spontaneous Ca$^{2+}$ transients (left panel) or Ca$^{2+}$ waves (right panel) in quiescent kl/kl cardiomyocytes. (F) Occurrence of SCR in +/+ ($n = 48$ cells/$N = 5$ mice) and kl/kl ($n = 39$ cells/$N = 5$ mice). (G) Line-scan images and fluorescence profiles of cardiomyocytes paced at 2-Hz field stimulation. (H) Occurrence of pro-arrhythmogenic events related to automatic Ca$^{2+}$ transients and automatic contractions in +/+ ($n = 26$ cells/$N = 5$ mice) and kl/kl ($n = 38$ cells/$N = 5$ mice) mice. Data are shown as mean ± SEM. [*]$P < 0.05$, significantly different from +/+ mice
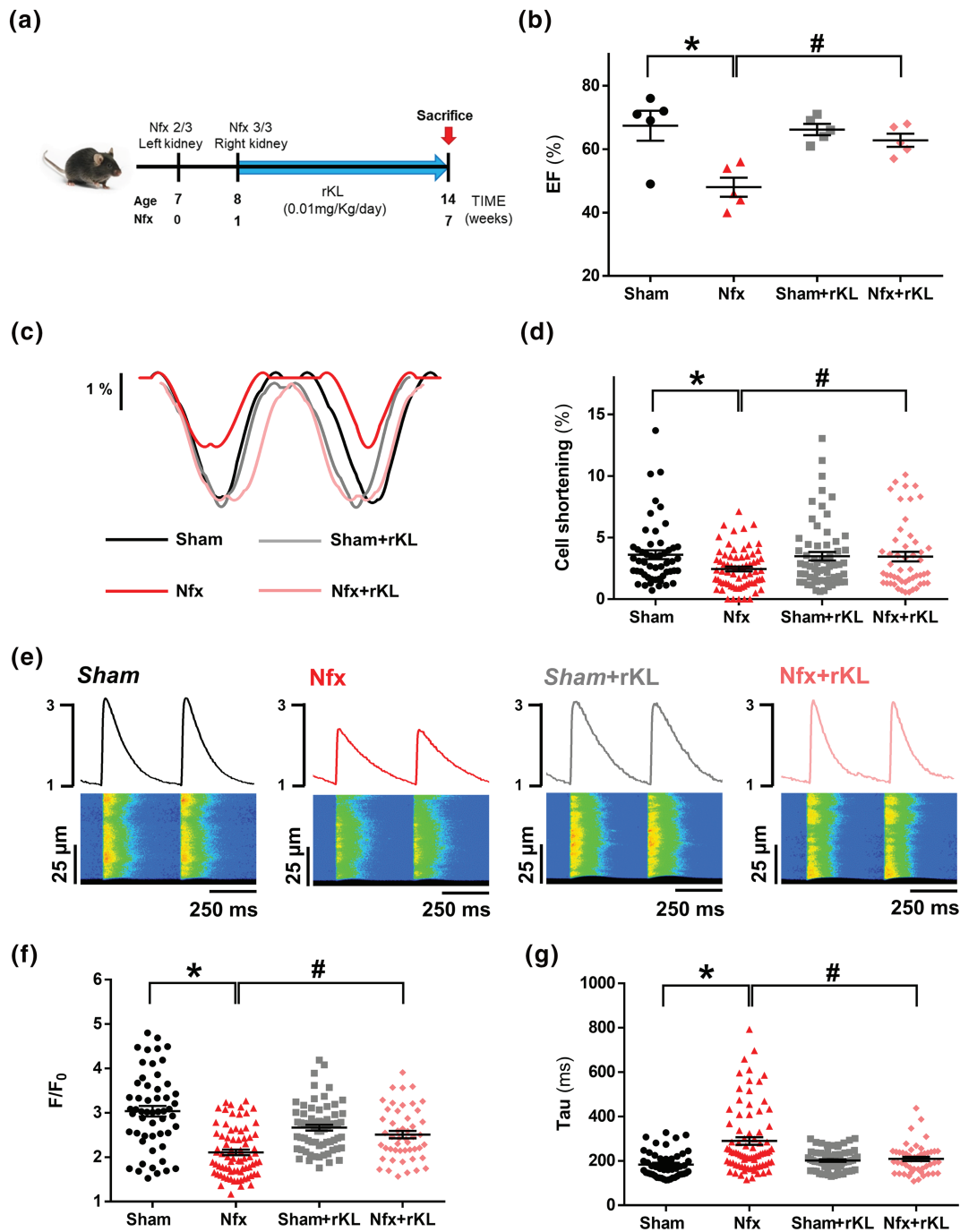
**FIGURE 3** Recombinant Klotho prevents contractile cellular dysfunction and reduction in systolic $Ca^{2+}$. (A) Schematic design of chronic kidney disease (CKD) animal model (5/6 nephrectomy) and treatments. (B) Mean values of ejection fraction (EF) from Sham ($N$ = 5 mice), Nfx ($N$ = 5 mice), Sham+rKL ($N$ = 5 mice), and Nfx+rKL ($N$ = 5 mice) mouse hearts. (C) Cell shortening profiles of cardiomyocytes. (D) Percentage of cell contraction of Sham ($n$ = 52 cells/$N$ = 5 mice), Nfx ($n$ = 73 cells/$N$ = 6 mice), Sham+rKL ($n$ = 62 cells/$N$ = 5 mice), and Nfx+rKL ($n$ = 48 cells/$N$ = 6 mice). (E) Line-scan images and fluorescence profiles of cardiomyocytes under 2-Hz field stimulation. (F and G) Mean values of peak ($F/F_0$) (F) and time of decay (*Tau*) (G) of electrically evoked $Ca^{2+}$ transients in Sham ($n$ = 54 cells/$N$ = 5 mice), Nfx ($n$ = 77 cells/$N$ = 6 mice), Sham+rKL ($n$ = 67 cells/$N$ = 5 mice), and Nfx+rKL ($n$ = 49 cells/$N$ = 6 mice). Data shown mean ± SEM. $^*P$ < 0.05, significantly different from Sham; $^\#P$ < 0.05, significantly different from Nfx

*col1a1* or *col3a1* expression levels by quantitative PCR in hearts from *Sham* and Nfx mice. No differences were detected between *Sham* and Nfx mice (1.031 ± 0.13 vs. 1.136 ± 0.11 arbitrary units, for *col1a1*; 1.058 ± 0.18 vs. 1.29 ± 0.11, for *col3a1*). Therefore, no signs of cardiac hypertrophy or fibrosis were detected in Nfx mice. Kidney function was impaired in Nfx mice, as demonstrated by significantly higher levels of plasma urea and BUN in the mice that underwent Nfx, compared with those in Sham mice (Table 2). These parameters remained elevated in rKL-treated Nfx mice, indicating that chronic rKL treatment did not restore renal function. FGF-23 levels were

**TABLE 2**  Macroscopic and biochemical parameters in an experimental CKD model

|  | Sham | Nfx | Sham+rKL | Nfx+rKL |
|---|---|---|---|---|
| *Macroscopic parameters* | | | | |
| Body weight (BW, g) | 27.5 ± 0.5 (N = 16) | 25.4 ± 0.6* (N = 20) | 27.2 ± 0.4 (N = 17) | 25.2 ± 0.6† (N = 22) |
| Heart weight (HW, mg) | 200.9 ± 6.2 (N = 16) | 187.7 ± 8.1 (N = 20) | 186.1 ± 3.9 (N = 17) | 185.6 ± 4.6 (N = 22) |
| HW/BW ratio | 7.31 ± 0.17 (N = 16) | 7.45 ± 0.21 (N = 20) | 6.80 ± 0.13 (N = 17) | 7.40 ± 0.17 (N = 22) |
| Kidney weight (KW, mg) | 165.9 ± 6.5 (N = 16) | 146.1 ± 6.2* (N = 20) | 165.9 ± 4.5 (N = 17) | 134.8 ± 4.5† (N = 22) |
| *Biochemical parameters* | | | | |
| Urea (mg·L$^{-1}$) | 516.1 ± 26.2 (N = 10) | 1103.7 ± 93.0* (N = 10) | 453.9 ± 47.6 (N = 10) | 1070.1 ± 91† (N = 10) |
| BUN (mg·L$^{-1}$) | 241.2 ± 12.2 (N = 10) | 515.4 ± 43.5* (N = 10) | 212.1 ± 22.2 (N = 10) | 500.0 ± 43† (N = 10) |
| Phosphorus (mg·L$^{-1}$) | 80.1 ± 9 (N = 10) | 72.2 ± 7 (N = 10) | 67.6 ± 7 (N = 10) | 79.0 ± 7 (N = 10) |
| FGF-23 (pg·ml$^{-1}$) | 144.6 ± 14.4 (N = 10) | 352.7 ± 41.7* (N = 10) | 138.6 ± 18.8 (N = 10) | 368.5 ± 39.5† (N = 10) |

*Note.* Data for macroscopic and biochemical parameters per experimental group are reported as mean ± SEM. BUN, blood urea nitrogen; BW, body weight; FGF-23, fibroblast growth factor 23; HW, heart weight; KW, kidney weight.

*$P < 0.05$, significantly different from Sham;

†$P < 0.05$, significantly different from Sham+rKL.

significantly elevated in Nfx mice, and also in Nfx animals chronically treated with rKL. By contrast, phosphorus levels were similar in all groups, likely due to the compensatory and rapid phosphaturic action evoked by the high FGF-23 levels. EF was measured by echocardiography as indicator of *in vivo* left ventricle global systolic function. EF was significantly reduced in Nfx mice, compared with Sham mice, whereas Nfx treated with rKL for 6 weeks exhibited significantly improved EF compared with that in Nfx treated with vehicle, which were not different from Sham+rKL mice (Figure 3b). Electrically evoked Ca$^{2+}$ transients of cardiomyocytes were studied under field stimulation of 2 Hz. Regarding contractile function, representative cell shortening profiles are shown for all groups in Figure 3c, and we observed a significant decrease in cardiomyocyte shortening in Nfx compared with Sham cells (Figure 3d). Whereas no effect of rKL was found in Sham cells for shortening, Nfx+rKL cells showed a significant increase in cell contraction, compared with vehicle-treated Nfx cardiomyocytes (Figure 3c, d). Figure 3e shows representative line-scan images (bottom panels) and fluorescence profiles (upper panels) corresponding to intracellular Ca$^{2+}$ transients in all experimental groups. Similar differences in the amplitude of Ca$^{2+}$ transients (F/F$_0$) were found between Sham and Nfx mice, analysed in cells or in hearts (3.04 ± 0.12 vs. 2.11 ± 0.06 or 3.18 ± 0.32, 2.12 ± 0.14, respectively). Ca$^{2+}$ transients amplitude (F/F$_0$) was significantly lower in Nfx cells than in Sham cells and was significantly higher in rKL-treated Nfx cells than in vehicle-treated Nfx cells (Figure 3f). Moreover, longer *Tau* values observed in Nfx cells (Figure 3g) indicate an impairment in SERCA2a function, which was also evident in the fluorescence profiles normalised to the peak of Ca$^{2+}$ transients obtained from Sham, compared with Nfx cells (Figure S7). Similarly, *K* SERCA2a was significantly lower in Nfx mice than in Sham mice (Figure S8). rKL treatment prevented the increase in *Tau* (Figure 3g). No differences were found for *Tau* in Sham+rKL and Nfx+rKL cardiomyocytes (Figure 3g). Thus, chronic rKL treatment prevented the cardiac dysfunction and impairment in cell shortening observed in Nfx cardiomyocytes.

## 3.3 | Increased diastolic Ca$^{2+}$ leak induced by experimental chronic kidney disease is prevented by recombinant Klotho administration

We evaluated SR-Ca$^{2+}$ load in experimental CKD and the effect of rKL treatment. Figure 4a shows representative line-scan images of caffeine-induced Ca$^{2+}$ release in each experimental group. CKD development led to a significant decrease in caffeine-evoked Ca$^{2+}$ transient amplitude (F/F$_0$) (Figure 4b), and this was partly prevented in rKL-treated Nfx mice (Figure 4b). We tested whether the diastolic Ca$^{2+}$ leak could be involved in the decreased SR-Ca$^{2+}$ content evident in CKD. We next analysed the diastolic Ca$^{2+}$ leak by measuring Ca$^{2+}$ spark frequency and SCR. Figure 4c shows line-scan examples of Ca$^{2+}$ spark recordings in the different groups of cardiomyocytes. Ca$^{2+}$ spark frequency was significantly higher in Nfx cardiomyocytes than in Sham cardiomyocytes (Figure 4d). This increase was not observed in cardiomyocytes from Nfx mice treated with rKL (Figure 4d). We also analysed diastolic SCR in the form of Ca$^{2+}$ waves (Figure 4e, left panel) and spontaneous Ca$^{2+}$ transients (Figure 4e, right panel). The occurrence of SCR was 1.8-fold higher in Nfx cardiomyocytes (as Ca$^{2+}$ spark frequency shown in Figure 4d) than in Sham cardiomyocytes (Figure 4f). However, chronic rKL treatment in Nfx mice prevented the increase of cardiomyocytes with SCR: 4% in rKL-treated Nfx mice and 20% in vehicle-treated Nfx mice (Figure 4f), which was even lower than that from Sham or rKL-treated Sham mice (12%, Figure 4f).

## 3.4 | Chronic recombinant Klotho treatment prevents pro-arrhythmogenic Ca$^{2+}$ events, RyR hyperactivity, and phosphorylation promoted by experimental chronic kidney disease
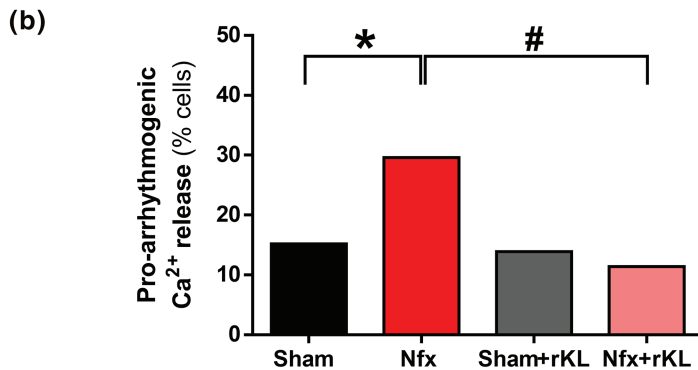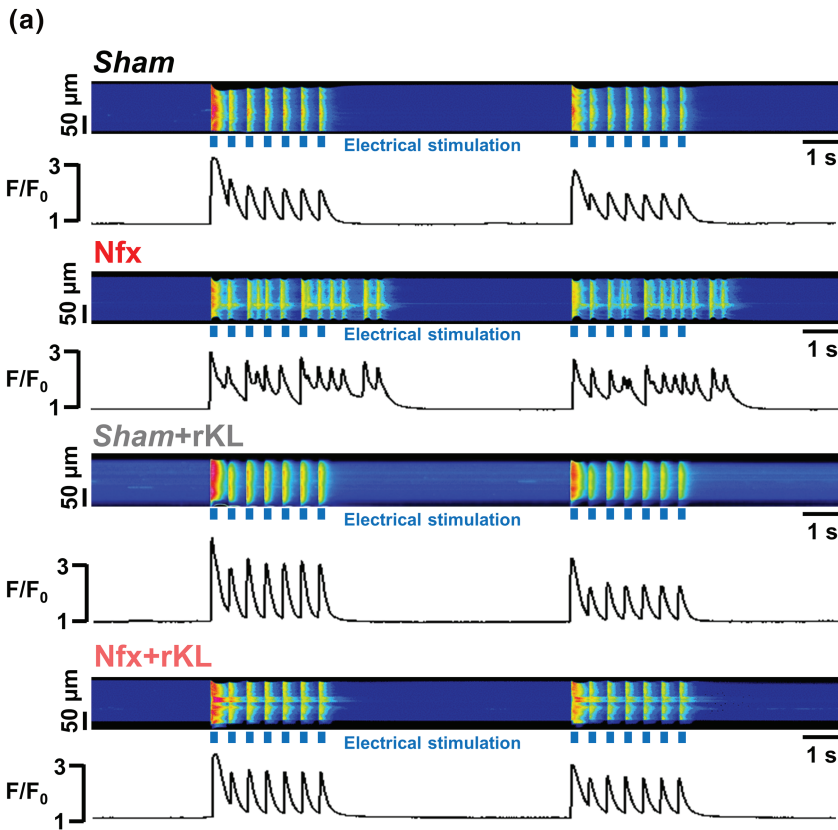
We examined for the presence of arrhythmic behaviour dependent on Ca$^{2+}$ cycling alterations during electrical pacing in the
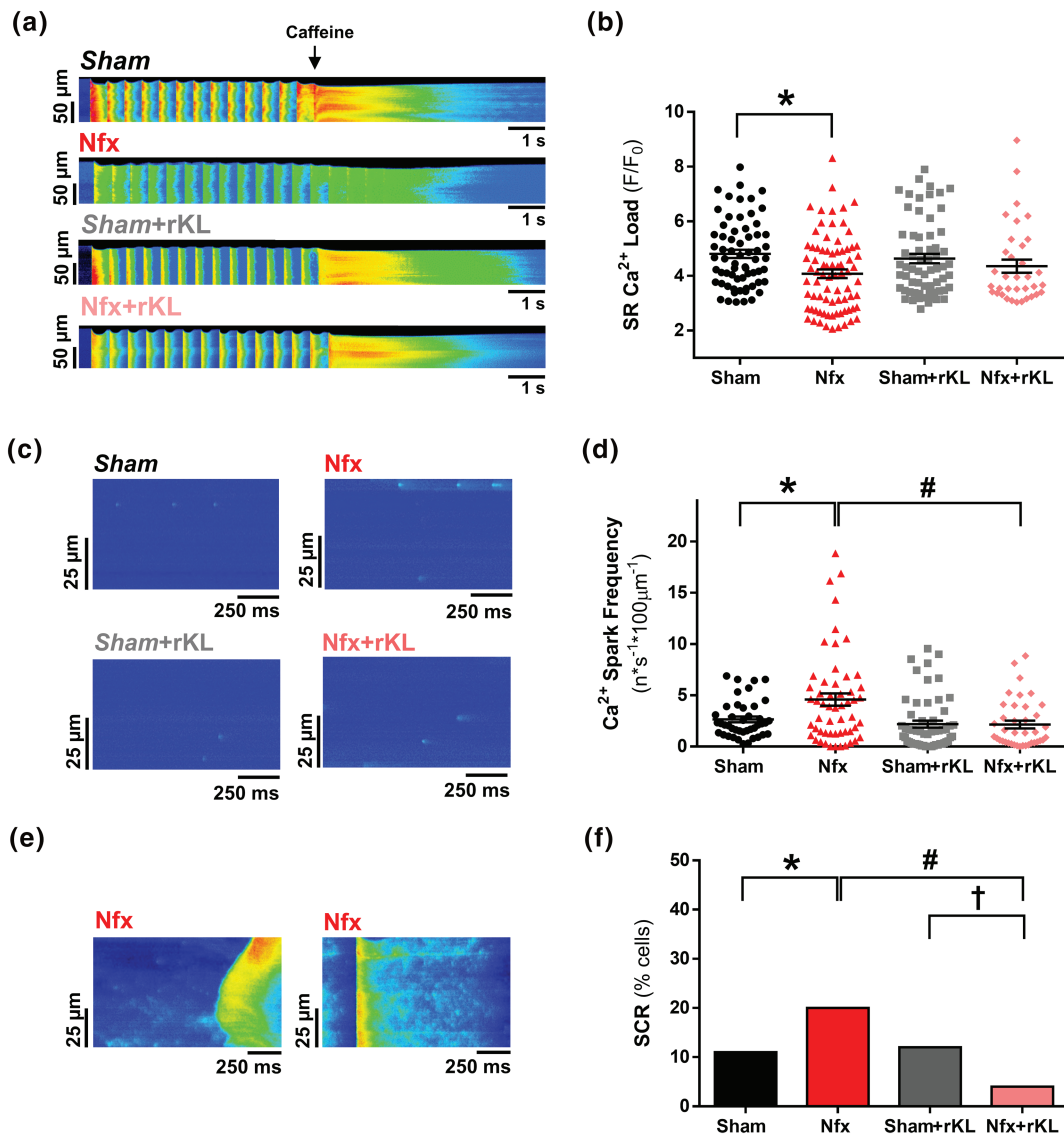
**FIGURE 4** Recombinant Klotho prevents SR-Ca$^{2+}$ load and diastolic SR-Ca$^{2+}$ leak in experimental chronic kidney disease (CKD). (A) Line-scan images of cardiomyocytes under 2-Hz field stimulation perfused with caffeine. (B) Mean values of caffeine-evoked Ca$^{2+}$ transients amplitude expressed as peak ($F/F_0$) in Sham ($n$ = 66 cells/$N$ = 6 mice), Nfx ($n$ = 79 cells/$N$ = 6 mice), Sham+rKL ($n$ = 67 cells/$N$ = 6 mice), and Nfx+rKL ($n$ = 49 cells/$N$ = 6 mice) cardiomyocytes. (C) Line-scan images of spark recordings in quiescent cardiomyocytes. (D) Mean values of Ca$^{2+}$ spark frequency in Sham (1,270 sparks, $n$ = 42 cells/$N$ = 5 mice), Nfx (2,985 sparks, $n$ = 55 cells/$N$ = 6 mice), Sham+rKL (1,188 sparks, $n$ = 56 cells/$N$ = 5 mice), and Nfx+rKL (1,075 sparks, $n$ = 39 cells/$N$ = 6 mice). (E) Line-scan images of spontaneous Ca$^{2+}$ release (SCR) as Ca$^{2+}$ waves (left panel) or spontaneous Ca$^{2+}$ transients (right panel) in quiescent Nfx cardiomyocytes. (F) Occurrence of SCR in Sham ($n$ = 42 cells/$N$ = 5 mice), Nfx ($n$ = 55 cells/$N$ = 6 mice), Sham+rKL ($n$ = 56 cells/$N$ = 5 mice), and Nfx+rKL ($n$ = 39 cells/$N$ = 6 mice) cardiomyocytes. Data are shown as mean ± SEM. *$P$ < 0.05, significantly different from Sham; #$P$ < 0.05, significantly different from Nfx; and †$P$ < 0.05, significantly different from Sham+rKL

experimental CKD model. Figure 5a shows representative line-scan Ca$^{2+}$ images of ventricular cardiomyocytes from Sham or Nfx mice, with or without rKL treatment and exposed to trains of electrical stimulation. When compared with Sham, Nfx cardiomyocytes presented a significant increase of automatic Ca$^{2+}$ transients triggering automatic contractions between electrical pulses and after electrical pacing, and this was prevented by rKL treatment (Figure 5b). Given these findings, we next assessed whether alterations in RyR sensitivity could explain the arrhythmic behaviour in experimental CKD. Considering that ryanodine binds only to open RyRs, we

determined the levels of functionally active RyRs in equivalent systolic and diastolic Ca$^{2+}$ conditions in vitro. During the systolic Ca$^{2+}$ recordings, we found a significant 2.9-fold increase in [$^3$H]-ryanodine binding in Nfx hearts (Figure 6a), and this activity was effectively decreased by rKL, although it did not reach the levels in Sham animals, suggesting that additional mechanisms (i.e., SR-Ca$^{2+}$ load) participate in decreasing the activity of RyRs. During diastolic Ca$^{2+}$ recordings, Nfx hearts showed a significant 3.2-fold increase in the binding of [$^3$H]-ryanodine at 100 nmol L$^{-1}$ of free [Ca$^{2+}$] (Figure 6b), and again, rKL treatment reduced the Ca$^{2+}$ sensitivity

**(a)**



**(b)**



**FIGURE 5** Recombinant Klotho treatment impedes pro-arrhythmogenic events induced by Nfx. (A) Line-scan images and fluorescence profiles of cardiomyocytes paced at 2-Hz field stimulation. (B) Occurrence of pro-arrhythmogenic events related to automatic $Ca^{2+}_I$ transients and automatic contractions in Sham ($n = 92$ cells/$N = 5$ mice), Nfx ($n = 142$ cells/$N = 6$ mice), Sham+rKL ($n = 72$ cells/$N = 5$ mice), and Nfx+rKL ($n = 149$ cells/$N = 7$ mice) mice. Data are shown as mean ± SEM. $^*P < 0.05$, significantly different from Sham; $^\#P < 0.05$, significantly different from Nfx

of RyRs in Nfx hearts (Figure 6b). As Nfx did not alter total RyR protein expression levels (Figure 6c and d, upper panels), the results indicate that RyRs from Nfx hearts are more sensitive to $Ca^{2+}$. To determine the mechanism involved in RyR hyperactivity, we examined the phosphorylation status of cardiac RyR at two serine residues: $Ser^{2030}$, key phosphorylation site for **protein kinase A (PKA)**, and $Ser^{2814}$, the specific phosphorylation site for **$Ca^2$$^+$/calmodulin-dependent protein kinase II (CaMKII)**. RyR phosphorylation at $Ser^{2030}$ and $Ser^{2814}$ was significantly higher in extracts from Nfx mice than from Sham mice (Figure 6c and d). This increased phosphorylation for $Ser^{2030}$ and $Ser^{2814}$ was not observed in Nfx mice treated with rKL, where basal levels of phosphorylation were similar to those of Sham mice.

### 3.5 | Klotho overexpression protects against cardiomyocyte contractile dysfunction and pro-arrhythmic $Ca^{2+}$ events in chronic kidney disease but does not eliminate renal damage

We used *Tg-Kl* mice to examine the cardioprotective role of endogenous Klotho overexpression in a uraemic context. Serum levels of BUN were significantly higher in *Tg-Kl* mice subjected to Nfx than Sham-*Tg-Kl* mice (Figure 7a). No differences were observed in serum phosphorus levels between both groups (Figure 7b), but serum FGF-23 levels were significantly higher in Nfx-*Tg-Kl* mice than in Sham-*Tg-Kl* mice (Figure 7c). Analysis of $Ca^{2+}$ cycling in isolated cardiomyocytes from both groups revealed no differences in $Ca^{2+}$
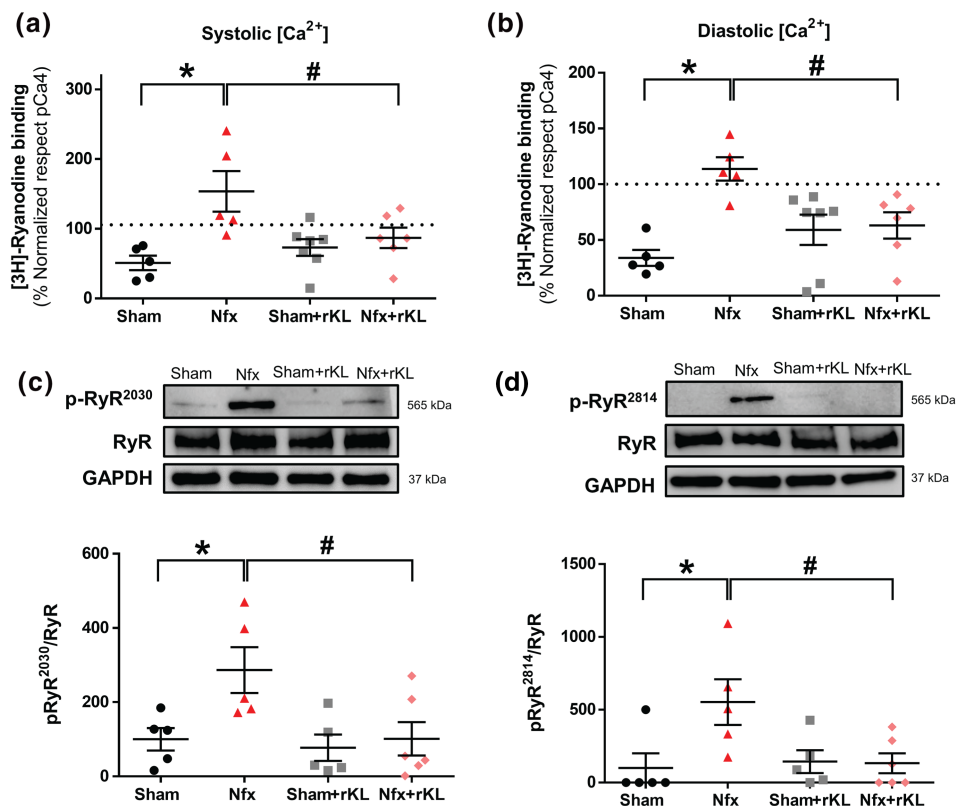
**FIGURE 6** Recombinant Klotho protects against RyR hyperactivation in experimental chronic kidney disease (CKD). (A and B) Specific [$^3$H]-ryanodine binding at (A) 10 μM (equivalent to the intracellular $Ca^{2+}$ rise in systole) and (B) 100 nM (equivalent to basal levels of intracellular $Ca^{2+}$ in quiescent conditions or diastole) and free $Ca^{2+}$ concentrations of heart homogenates from Sham ($N = 5$ mice), Nfx ($N = 5$ mice), Sham+rKL ($N = 7$ mice), and Nfx+rKL ($N = 6$ mice). [$^3$H]-Ryanodine binding values were normalised to the specific [$^3$H]-ryanodine binding at 100 μmol $L^{-1}$ of free [$Ca^{2+}$]. (C and D) Western blots (upper panels) and quantification (bottom panels) of RyR phosphorylation at $Ser^{2030}$ (p-RyR$^{2030}$) or at $Ser^{2814}$ (p-RyR$^{2814}$) normalised to total RyR from Sham ($N = 5$ mice), Nfx ($N = 7$ mice), Sham+rKL ($N = 5$ mice), and Nfx+rKL ($N = 7$ mice) hearts. Data are shown as mean ± SEM. $^*P < 0.05$ significantly different from Sham; $^\#P < 0.05$, significantly different from Nfx

spark frequency (Figure 7d), SCR (Figure 7e), SR $Ca^{2+}$ load (Figure 7f), intracellular $Ca^{2+}$ transients (Figure 7g), or cell shortening (Figure 7h) between them. Overall, these results show that endogenous Klotho overexpression protects against changes in $Ca^{2+}$ cycling, preventing contractile dysfunction and diastolic pro-arrhythmogenic $Ca^{2+}$ release in Nfx mice.

## 4 | DISCUSSION

Klotho was initially discovered as an age-suppressing gene in mice that extends lifespan when overexpressed (Kuro-o et al., 1997). Klotho is expressed mainly in the kidney and is composed of a very short intracellular domain, a transmembrane domain, and a large extracellular domain that is susceptible to ectodomain shedding, resulting in two forms, membrane and secreted or sKL (Kuro-o, 2011a). In the kidney, membrane Klotho acts as a co-receptor for FGF-23, increasing the affinity of FGFRs for FGF-23-mediated phosphaturic actions (Urakawa et al., 2006). sKL is a humoral factor with pleiotropic functions, including a cardioprotective action through the regulation of ion channels (Xie et al., 2012) that is independent of

FGF-23 and phosphate (Xie et al., 2015). CKD is considered a Klotho-deficient state (Asai et al., 2012; Kuro-O, 2011b). CKD is accompanied by premature aging and is considered a global health concern, because of its high prevalence of around 10% in the general population (Coresh et al., 2007). At the experimental level, models of premature aging, such as Klotho-hypomorphic mice, develop early-stage CKD. In addition, other authors have recently described that uremic environment increases with aging in the experimental CKD model (Heveran et al., 2019). However, no studies have described overlapping effects of CKD and aging on cardiac function. Cardiac dysfunction and fatal arrhythmias, in many cases asymptomatic ventricular arrhythmias, are the leading causes of mortality in patients with CKD, especially in those with end-stage renal disease (Banerjee, 2016; Verde et al., 2016). However, the underlying mechanisms involved in this cardiorenal interaction remain to be defined and clinicians remain uncertain about how to reduce the burden of cardiovascular events in CKD.

Our study provides the first demonstration, to our knowledge, that experimental uraemia induced by Klotho deficiency or nephrectomy with reduced Klotho levels is linked to a strong defect in $Ca^{2+}$ handling, characterised by decreased systolic $Ca^{2+}$ release and
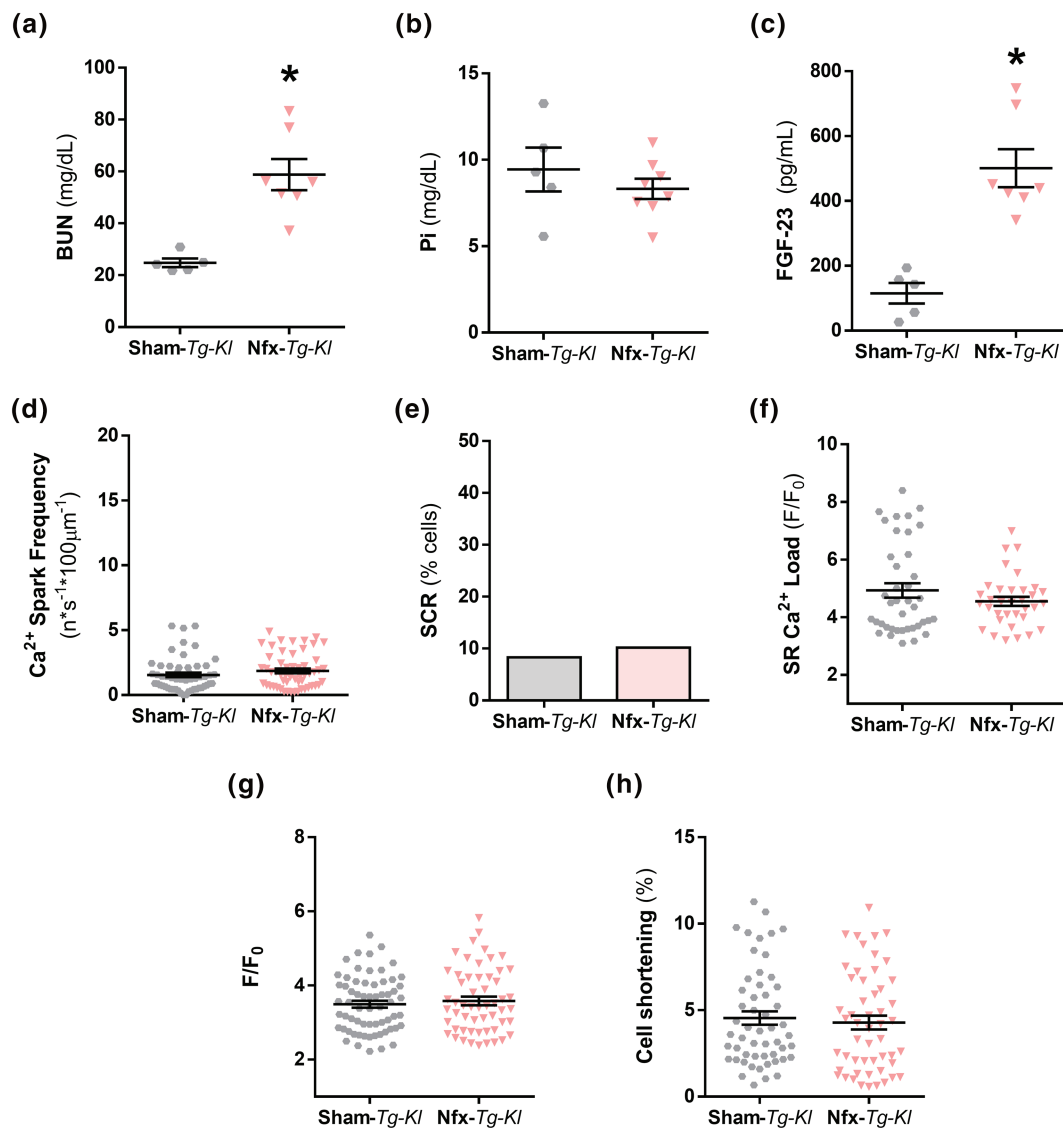
**FIGURE 7** Klotho overexpression protects from electrical cardiac and $Ca^{2+}$ cycling alterations induced by chronic kidney disease (CKD). (A–C) Mean serum levels of (A) blood urea nitrogen (BUN), (B) phosphates (Pi), and (C) fibroblast growth factor-23 (FGF-23) in Sham-*Tg-Kl* (*N* = 5 mice) and Nfx-*Tg-Kl* (*N* = 7 mice). (D) Mean values of $Ca^{2+}$ spark frequency in Sham-*Tg-Kl* (995 sparks, *n* = 54 cells/*N* = 5 mice) and Nfx-*Tg-Kl* (893 sparks, *n* = 55 cells/*N* = 6 mice). (E) Occurrence of SCR in Sham-*Tg-Kl* (*n* = 54 cells/*N* = 5 mice) and Nfx-*Tg-Kl* (*n* = 55 cells/*N* = 6 mice). (F) Mean values of caffeine-evoked $Ca^{2+}$ transients amplitude expressed as peak ($F/F_0$) in Sham-*Tg-Kl* (*n* = 40 cells/*N* = 5 mice) and Nfx-*Tg-Kl* (*n* = 34 cells/*N* = 6 mice). (G) Mean values of peak ($F/F_0$) of electrically evoked $Ca^{2+}$ transients in Sham-*Tg-Kl* (*n* = 64 cells/*N* = 5 mice) and Nfx-*Tg-Kl* (*n* = 55 cells/*N* = 6 mice). (H) Percentage of cell contraction of Sham-*Tg-Kl* (*n* = 56 cells/*N* = 5 mice) and Nfx-*Tg-Kl* (*n* = 52 cells/*N* = 6 mice). Data are shown as mean ± SEM. *$P < 0.05$, significantly different from Sham-*Tg-Kl*

contractile dysfunction and increased diastolic pro-arrhythmogenic $Ca^{2+}$ release and leak, accompanied by RyR hyperactivity. Our data also support the concept that preserving Klotho availability, exogenously using prophylactic chronic treatment with rKL or endogenously enhancing Klotho expression, could be potential therapeutic strategies to protect the heart from the uraemic environment, including alterations in intracellular $Ca^{2+}$ cycling that trigger contractile dysfunction and pro-arrhythmic mechanisms such as the hyperactivation of RyRs observed in CKD (see Graphical Abstract). Our results show an increase in RyR activity in Nfx mice with higher spontaneous diastolic $Ca^{2+}$ release and a diminution in SR-$Ca^{2+}$ load. Both mechanisms are

known to be associated with cardiac dysfunction and the predisposition to arrhythmias. The decrease in systolic $Ca^{2+}$ release accompanied by a worsened contractile response, concomitant with extra-contractions, and $Ca^{2+}$ leak in the form of $Ca^{2+}$ sparks and waves during diastole were pro-arrhythmic $Ca^{2+}$ events in cardiomyocytes from *kl/kl* and CKD mice. Furthermore, we identified a CKD-related increase in RyR phosphorylation as an underlying molecular explanation for the high RyR activity. Accordingly, RyR was robustly phosphorylated at its PKA (3-fold higher) and CaMKII (5-fold higher) sites in CKD mice. Similar results of PKA-mediated and CaMKII-mediated RyR phosphorylation and its relationship with the

predisposition to trigger fatal ventricular arrhythmias have also been found in experimental models of heart failure (Grimm et al., 2015; Xiao et al., 2005). This post-translational RyR modification of increased phosphorylation can be explained by the higher $Ca^{2+}$ sensitivity of RyR at systolic and diastolic $Ca^{2+}$ concentrations in CKD mice, which was prevented by rKL administration. Dhindwal et al. proposed that phosphorylation induces RyR to adopt a protein conformation that requires less energy for the transition to the open state (Dhindwal et al., 2017). Therefore, a more flexible RyR conformation might exist when the phosphorylation state is significantly increased, as in CKD mice, in both phosphorylation sites ($Ser^{2030}$ and $Ser^{2814}$). Moreover, a similar increase in $Ca^{2+}$ sensitivity has been observed in ventricular arrhythmia in experimental catecholaminergic polymorphic ventricular tachycardia (Fernández-Velasco et al., 2009). Gender-related differential activation of PKA and CaMKII pathways exists in rodent hearts also under pathological conditions (Bell et al., 2015; Parks, Ray, Bienvenu, Rose, & Howlett, 2014). For example, in diabetic cardiomyopathy, the contribution of PKA-dependent and CaMKII-dependent pathways is less relevant in female mice than in male mice, with a significant diminution of PKA-induced and CaMKII-induced RyR phosphorylation sites correlating with decreased spark-mediated calcium leak in female mice (Delgado, Gomez, Samia El Hayek, Ruiz-Hurtado, & Pereira, 2019; Pereira et al., 2014). Thus, it would be very likely that these pathways could be also less active in female mice than in male mice, in the setting of uremic cardiomyopathy. However, in our study, female mice were not studied, to avoid the potential cardioprotective effects mediated by oestrogens, which could be overlapping the Klotho-mediated cardioprotective actions in experimental conditions of CKD. Further experimental studies are needed to assess the contribution of oestrogens to the $Ca^{2+}$ mishandling observed under uremic cardiomyopathy conditions.

This study has several potential clinical and therapeutic applications for renal patients. First, our results show that decreased Klotho availability, together with the presence of pathologically elevated FGF-23 levels, might be a warning sign for increased risk of developing arrhythmic events in patients with CKD. Supporting this idea, several studies have previously shown that FGF-23 exposure alters cardiac contractility and $Ca^{2+}$ handling in isolated adult ventricular cardiomyocytes (Navarro-García et al., 2019; Touchberry et al., 2013) and in HL-1 atrial cells (Kao et al., 2014). These findings support the notion that systemic elevation of FGF-23 is likely to have deleterious and direct effects on heart function in the complex pathological setting of uraemic cardiomyopathy (Faul, 2018). However, in the clinical setting, further studies are still needed to establish whether FGF-23 itself is an independent uremic factor able to play a relevant role in the cardiac events accompanying the decline of renal function. Accordingly, a logical experimental approach would be the use of FGF-23 blocking antibodies as the most direct strategy to inhibit FGF-23 actions in the uraemic context. Yet in a preclinical model of CKD, rats treated with a neutralising FGF-23 antibody presented elevated systemic serum phosphate and developed severe cardiovascular complications (Shalhoub et al., 2012). Thus, the key point would be not to fully suppress FGF-23 actions, such as the physiological

phosphaturic action, but only to block its damaging actions on the heart. The second application would involve exogenous Klotho administration as a therapeutic option to block the deleterious FGF-23 actions on the heart. Klotho is emerging as a potential cardioprotective factor for uraemic cardiomyopathy. Indeed, Klotho protects against vascular calcification in human (Lim et al., 2012) and experimental models (Hu et al., 2011) of CKD. Moreover, sKL deficiency in CKD seems to render the myocardium more susceptible to stress-induced injury (Xie et al., 2012). Similarly, some authors have proposed that FGF-23 induces cardiac toxicity only when serum levels of sKL are reduced in CKD (Hu et al., 2015), whereas other authors posit that Klotho prevents uraemic cardiomyopathy by a direct effect on cardiomyocytes independently of FGF-23 and phosphates (Xie et al., 2015). Nevertheless, clinical studies on the predictive value of Klotho have produced conflicting results, with some reporting that plasma sKL levels did not predict cardiovascular events or death in a large CKD cohort (Seiler et al., 2013), while others demonstrated a clear association between preserved sKL levels and reduced cardiovascular morbidity and mortality in dialysis-dependent CKD (Hu et al., 2011). The idea that sKL could function as a decoy of FGF-23 actions in the heart is in agreement with our results. Thus, we observed a cardioprotective effect of rKL administration on preventing contractile dysfunction and diastolic $Ca^{2+}$ leak related to pro-arrhythmic events in cardiomyocytes from Nfx mice. In this respect, Klotho has been shown to produce beneficial cardiac actions on ionic channels, including the downregulation of **TRPC6 channels** in conditions of cardiac hypertrophy (Xie et al., 2012; Xie et al., 2015). However, in physiological conditions, the contribution of TRPC6 channels to the total $Ca^{2+}$ entry in cardiomyocytes is small and is higher in conditions of cardiac hypertrophy. In the present study, we found no evidence of cardiac morphology changes such as hypertrophy or fibrosis in Klotho-hypomorphic mice and mice after 6 weeks of 5/6 nephrectomy. The kl/kl mice showed an increase in HW/BW ratio that was not accompanied by an increase in cardiomyocyte area, or ANP and collagen expression as specific markers of cellular hypertrophy or fibrosis, respectively. A possible explanation for these results is that Klotho-hypomorphic mice showed reduced BW compared with +/+ mice and they also present an important growth retardation affecting all organs, which could explain the reduced cardiomyocyte areas or collagen levels, compared with their +/+ littermates. Besides, the absence of Klotho expression also induces important ectopic calcification in arterial walls and cardiac muscle (Kuro-o et al., 1997; Yoshida, Fujimori, & Nabeshima, 2002). All these facts might favour a higher HW/BW ratio than that expected for its body weight and animal size. Therefore, these results support the conclusion that $Ca^{2+}$ mishandling observed in kl/kl mice is not due to cardiomyocyte hypertrophy or deleterious remodelling development, although the influence of systemic calcaemia and alterations in vitamin D homeostasis in this Klotho mutant mice (Yoshida et al., 2002) could not be discarded, especially on the elevated diastolic $Ca^{2+}$ release and pro-arrhythmic events of kl/kl cardiomyocytes.

In general, the experimental CKD model shows a compromised EF and cardiac dysfunction in mice (Bro, Bollano, Brüel, Olgaard, &

Nielsen, 2008; Chen et al., 2017). However, there are apparently opposite results related to hypertrophy development that might appear together with this cardiac dysfunction. Thus, some authors have described Nfx-induced cardiac dysfunction with a significant increment of the heart weight (Chen et al., 2017), while other authors using the same experimental CKD model did not observe any increase in the heart weight (Bro et al., 2008) as we have also observed in the present study. These apparently opposing results could be explained by the age of the animals used and also the time employed from 5/6 Nfx surgery to the cardiac analysis. In our hands, this experimental model of CKD developed a dysfunctional cardiac phenotype without hypertrophy or fibrosis development. This is an ideal *in vivo* model to study functional cardiac events such as heart failure and the predisposition to arrhythmia related to $Ca^{2+}$ mishandling in the context of uraemic cardiomyopathy without any overlap due to structural myocardial alterations. Using this model, we have demonstrated a cardioprotective role of Klotho through the normalisation of cardiomyocyte $Ca^{2+}$ cycling. Mechanistically, we propose that RyRs are a novel target of Klotho, and Klotho could act as a "brake" for the pro-arrhythmogenic $Ca^{2+}$ leak from the SR by impeding phosphorylation and hyperactivation of RyRs previously observed in CKD. By halting $Ca^{2+}$ leakage, Klotho helps to maintain an adequate cellular shortening due to the recovery of systolic $Ca^{2+}$ release in the form of $Ca^{2+}$ transients and, at the same time, impedes the increase in diastolic $Ca^{2+}$ release in the form of $Ca^{2+}$ sparks or waves that might favour reaching a intracellular $Ca^{2+}$ threshold able to evoke automatic $Ca^{2+}$ transients and extra-contractions. Finally, one of the most relevant findings of our study is that we show for the first time that Klotho can protect the heart from $Ca^{2+}$ mishandling associated with CKD, without any associated improvement in renal dysfunction. Thus, Nfx mice overexpressing Klotho or chronically treated with rKL present the same high systemic levels of FGF-23 and BUN as those Nfx mice treated with vehicle. We believe these findings are clinically relevant because strategies directed to maintain adequate Klotho levels could be a new therapeutic goal to directly protect the heart from a uraemic environment and guaranteeing FGF-23 phosphaturic action.

One limitation of the present study is the lack of data in larger animal models that exhibit closer physiological characteristics to humans, such as rabbits or pigs. Moreover, further investigation will be required to determine, in detail, whether the Klotho deficiency, a very common aspect in CKD patients, might influence diastolic $Ca^{2+}$ levels and therefore compromise cardiac contractility. We envision the need to corroborate the cardioprotective role of Klotho throughout the development of renal disease from initial stages, including the use of larger animal models in further studies.

In conclusion, this study has provided new insights into how Klotho availability determines cardiac function in uraemic cardiomyopathy via regulation of $Ca^{2+}$ handling. The present investigation revealed the dysregulated cardiac physiological mechanisms in uraemia modelled by Klotho deficiency or nephrectomy, including defects in systolic $Ca^{2+}$ release and contractile dysfunction together with RyR hyperactivation, which can explain the elevated presence of pro-arrhythmogenic $Ca^{2+}$ events found in a uraemic setting. All of these alterations in $Ca^{2+}$

handling observed in CKD mice were prevented when Klotho was present, indicating that therapeutic strategies directed to improve Klotho availability might be an effective approach to protecting the heart from cardiac dysfunction and arrhythmogenic potential events in CKD.

## AUTHOR CONTRIBUTIONS

G.R.-H. and J.A.N.-G. designed and conceptualised the experiments. J.A.N.-G., T.R.-G., and G.R.-H. performed the experiments. J.A.N.-G., A.R., T.R.-G., E.R.-S., L.G.-L., and G.R.-H. analysed the data. C.Z. carried out, analysed, and interpreted the echocardiograms. G.R.-H., M.F.-V., L.M.R., and M.K. provided reagents and materials. J.A.N.-G., M.F.-V., L.M.R., and M.K. helped with data interpretation. J.A.N.-G. and G.R.-H. wrote the manuscript.

## CONFLICT OF INTEREST

The authors declare no conflicts of interest.

## DECLARATION OF TRANSPARENCY AND SCIENTIFIC RIGOUR

This Declaration acknowledges that this paper adheres to the principles for transparent reporting and scientific rigour of preclinical research as stated in the *BJP* guidelines for Design & Analysis, Immunoblotting and Immunochemistry and Animal Experimentation, and as recommended by funding agencies, publishers, and other organisations engaged with supporting research.

## ORCID

*José Alberto Navarro-García* https://orcid.org/0000-0002-0317-4888

*Elena Rodríguez-Sánchez* https://orcid.org/0000-0002-5020-949X

*Gema Ruiz-Hurtado* https://orcid.org/0000-0003-3482-0915

## REFERENCES

Alexander, S. P. H., Fabbro, D., Kelly, E., Mathie, A., Peters, J. A., Veale, E. L., ... CGTP Collaborators. (2019a). THE CONCISE GUIDE TO PHARMACOLOGY 2019/20: Catalytic receptors. *British Journal of Pharmacology*, 176, S247–S296. https://doi.org/10.1111/bph.14751

Alexander, S. P. H., Fabbro, D., Kelly, E., Mathie, A., Peters, J. A., Veale, E. L., ... CGTP Collaborators. (2019b). THE CONCISE GUIDE TO PHARMACOLOGY 2019/20: Enzymes. *British Journal of Pharmacology*, *176*, S297–S396. https://doi.org/10.1111/bph.14752

Alexander, S. P. H., Kelly, E., Mathie, A., Peters, J. A., Veale, E. L., Armstrong, J. F., ... CGTP Collaborators. (2019). THE CONCISE GUIDE TO PHARMACOLOGY 2019/20: Transporters. *British Journal of Pharmacology*, *176*, S397–S493. https://doi.org/10.1111/bph.14753

Alexander, S. P. H., Mathie, A., Peters, J. A., Veale, E. L., Striessnig, J., Kelly, E., ... CGTP Collaborators. (2019). THE CONCISE GUIDE TO PHARMACOLOGY 2019/20: Ion channels. *British Journal of Pharmacology*, *176*, S142–S228. https://doi.org/10.1111/bph.14749

Alexander, S. P. H., Roberts, R. E., Broughton, B. R. S., Sobey, C. G., George, C. H., Stanford, S. C., ... Ahluwalia, A. (2018). Goals and practicalities of immunoblotting and immunohistochemistry: A guide for submission to the British Journal of Pharmacology. *British Journal of Pharmacology*, *175*, 407–411. https://doi.org/10.1111/bph.14112

Asai, O., Nakatani, K., Tanaka, T., Sakan, H., Imura, A., Yoshimoto, S., ... Saito, Y. (2012). Decreased renal α-Klotho expression in early diabetic nephropathy in humans and mice and its possible role in urinary calcium excretion. *Kidney International*, *81*, 539–547. https://doi.org/10.1038/ki.2011.423

Banerjee, D. (2016). Sudden cardiac death in haemodialysis: Clinical epidemiology and mechanisms. *Journal of Electrocardiology*, *49*, 843–847. https://doi.org/10.1016/j.jelectrocard.2016.07.016

Bell, J. R., Raaijmakers, A. J., Curl, C. L., Reichelt, M. E., Harding, T. W., Bei, A., ... Delbridge, L. M. (2015). Cardiac CaMKIIδ splice variants exhibit target signaling specificity and confer sex-selective arrhythmogenic actions in the ischemic-reperfused heart. *International Journal of Cardiology*, *181*, 288–296. https://doi.org/10.1016/j.ijcard.2014.11.159

Bergmark, B. A., Udell, J. A., Morrow, D. A., Jarolim, P., Kuder, J. F., Solomon, S. D., ... Sabatine, M. S. (2019). Klotho, fibroblast growth factor-23, and the renin-angiotensin system—an analysis from the PEACE trial. *European Journal of Heart Failure*, *21*, 462–470. https://doi.org/10.1002/ejhf.1424

Bers, D. M. (2002). Cardiac excitation–contraction coupling. *Nature*, *415*, 198–205. https://doi.org/10.1038/415198a

Bers, D. M. (2014). Cardiac sarcoplasmic reticulum calcium leak: Basis and roles in cardiac dysfunction. *Annual Review of Physiology*, *76*, 107–127. https://doi.org/10.1146/annurev-physiol-020911-153308

Bode, E. F., Briston, S. J., Overend, C. L., O'Neill, S. C., Trafford, A. W., & Eisner, D. A. (2011). Changes of SERCA activity have only modest effects on sarcoplasmic reticulum $Ca^{2+}$ content in rat ventricular myocytes. *The Journal of Physiology*, *589*, 4723–4729. https://doi.org/10.1113/jphysiol.2011.211052

Bro, S., Bollano, E., Brüel, A., Olgaard, K., & Nielsen, L. B. (2008). Cardiac structure and function in a mouse model of uraemia without hypertension. *Scandinavian Journal of Clinical and Laboratory Investigation*, *68*, 660–666. https://doi.org/10.1080/00365510802037272

Charytan, D. M., Foley, R., McCullough, P. A., Rogers, J. D., Zimetbaum, P., Herzog, C. A., ... MiD Investigators and Committees. (2016). Arrhythmia and sudden death in hemodialysis patients: protocol and baseline characteristics of the monitoring in dialysis study. *Clinical Journal of the American Society of Nephrology*, *11*, 721–734. https://doi.org/10.2215/CJN.09350915

Chen, J., Kieswich, J. E., Chiazza, F., Moyes, A. J., Gobbetti, T., Purvis, G. S., ... Collino, M. (2017). IκB kinase inhibitor attenuates sepsis-induced cardiac dysfunction in CKD. *Journal of the American Society of Nephrology*, *28*, 94–105. https://doi.org/10.1681/ASN.2015060670

Cheng, H., Song, L. S., Shirokova, N., González, A., Lakatta, E. G., Ríos, E., ... Stern, M. D. (1999). Amplitude distribution of calcium sparks in confocal images: Theory and studies with an automatic detection method. *Biophysical Journal*, *76*, 606–617. https://doi.org/10.1016/S0006-3495(99)77229-2

Coll, M., Ferrer-Costa, C., Pich, S., Allegue, C., Rodrigo, E., Fernández-Fresnedo, G., ... Brugada, R. (2018). Role of genetic and electrolyte abnormalities in prolonged QTc interval and sudden cardiac death in end-stage renal disease patients. *PLoS ONE*, *13*, e0200756. https://doi.org/10.1371/journal.pone.0200756

Coresh, J., Selvin, E., Stevens, L. A., Manzi, J., Kusek, J. W., Eggers, P., ... Levey, A. S. (2007). Prevalence of chronic kidney disease in the United States. *JAMA*, *298*, 2038–2047. https://doi.org/10.1001/jama.298.17.2038

Curtis, M. J., Alexander, S. P. H., Cirino, G., Docherty, J. R., George, C. H., Giembycz, M. A., ... Ahluwalia, A. (2018). Experimental design and analysis and their reporting II: updated and simplified guidance for authors and peer reviewers. *British Journal of Pharmacology*, *175*, 987–993. https://doi.org/10.1111/bph.14153

de Alba-Aguayo, D. R., Pavón, N., Mercado-Morales, M., Miranda-Saturnino, M., López-Casamichana, M., Guerrero-Hernández, A., ... Rueda, A. (2017). Increased calcium leak associated with reduced calsequestrin expression in hyperthyroid cardiomyocytes. *Cell Calcium*, *62*, 29–40. https://doi.org/10.1016/j.ceca.2017.01.009

Delgado, C., Gomez, A. M., Samia El Hayek, M., Ruiz-Hurtado, G., & Pereira, L. (2019). Gender-dependent alteration of Ca. *Frontiers in Physiology*, *10*, 40. https://doi.org/10.3389/fphys.2019.00040

Dhindwal, S., Lobo, J., Cabra, V., Santiago, D. J., Nayak, A. R., Dryden, K., & Samsó, M. (2017). A cryo-EM-based model of phosphorylation- and FKBP12.6-mediated allosterism of the cardiac ryanodine receptor. *Science Signaling*, *10*(480), eaai8842. https://doi.org/10.1126/scisignal.aai8842

Faul, C. (2018). FGF23 effects on the heart-levels, time, source, and context matter. *Kidney International*, *94*, 7–11. https://doi.org/10.1016/j.kint.2018.03.024

Fernández-Velasco, M., Rueda, A., Rizzi, N., Benitah, J. P., Colombi, B., Napolitano, C., ... Gómez, A. M. (2009). Increased $Ca^{2+}$ sensitivity of the ryanodine receptor mutant RyR2R4496C underlies catecholaminergic polymorphic ventricular tachycardia. *Circulation Research*, *104*, 201–209212p following 209. https://doi.org/10.1161/CIRCRESAHA.108.177493

Gagnon, R. F., & Gallimore, B. (1988). Characterization of a mouse model of chronic uremia. *Urological Research*, *16*, 119–126. https://doi.org/10.1007/BF00261969

Go, A. S., Chertow, G. M., Fan, D., McCulloch, C. E., & Hsu, C. Y. (2004). Chronic kidney disease and the risks of death, cardiovascular events, and hospitalization. *The New England Journal of Medicine*, *351*, 1296–1305. https://doi.org/10.1056/NEJMoa041031

Grimm, M., Ling, H., Willeford, A., Pereira, L., Gray, C. B., Erickson, J. R., ... Brown, J. H. (2015). CaMKIIδ mediates β-adrenergic effects on RyR2 phosphorylation and SR Ca(2+) leak and the pathophysiological response to chronic β-adrenergic stimulation. *Journal of Molecular and Cellular Cardiology*, *85*, 282–291. https://doi.org/10.1016/j.yjmcc.2015.06.007

Gutiérrez, O. M., Mannstadt, M., Isakova, T., Rauh-Hain, J. A., Tamez, H., Shah, A., ... Wolf, M. (2008). Fibroblast growth factor 23 and mortality among patients undergoing hemodialysis. *The New England Journal of Medicine*, *359*, 584–592. https://doi.org/10.1056/NEJMoa0706130

Herzog, C. A., Asinger, R. W., Berger, A. K., Charytan, D. M., Díez, J., Hart, R. G., ... Ritz, E. (2011). Cardiovascular disease in chronic kidney disease. A clinical update from Kidney Disease: Improving Global Outcomes (KDIGO). *Kidney International*, *80*, 572–586. https://doi.org/10.1038/ki.2011.223

Heveran, C. M., Schurman, C. A., Acevedo, C., Livingston, E. W., Howe, D., Schaible, E. G., ... Ferguson, V. L. (2019). Chronic kidney disease and aging differentially diminish bone material and microarchitecture in C57Bl/6 mice. *Bone*, *127*, 91–103. https://doi.org/10.1016/j.bone.2019.04.019

Hu, M. C., Shi, M., Cho, H. J., Adams-Huet, B., Paek, J., Hill, K., ... Moe, O. W. (2015). Klotho and phosphate are modulators of

pathologic uremic cardiac remodeling. *Journal of the American Society of Nephrology*, *26*, 1290–1302. https://doi.org/10.1681/ASN.2014050465

Hu, M. C., Shi, M., Gillings, N., Flores, B., Takahashi, M., Kuro-O, M., & Moe, O. W. (2017). Recombinant α-Klotho may be prophylactic and therapeutic for acute to chronic kidney disease progression and uremic cardiomyopathy. *Kidney International*, *91*, 1104–1114. https://doi.org/10.1016/j.kint.2016.10.034

Hu, M. C., Shi, M., Zhang, J., Quiñones, H., Griffith, C., Kuro-o, M., ... Moe, O. W. (2011). Klotho deficiency causes vascular calcification in chronic kidney disease. *Journal of the American Society of Nephrology*, *22*, 124–136. https://doi.org/10.1681/ASN.2009121311

Isakova, T., Cai, X., Lee, J., Xie, D., Wang, X., Mehta, R., ... Chronic Renal Insufficiency Cohort (CRIC) Study Investigators. (2018). Longitudinal FGF23 trajectories and mortality in patients with CKD. *Journal of the American Society of Nephrology*, *29*, 579–590. https://doi.org/10.1681/ASN.2017070772

Isakova, T., Xie, H., Yang, W., Xie, D., Anderson, A. H., Scialla, J., ... Chronic Renal Insufficiency Cohort (CRIC) Study Group. (2011). Fibroblast growth factor 23 and risks of mortality and end-stage renal disease in patients with chronic kidney disease. *JAMA*, *305*, 2432–2439. https://doi.org/10.1001/jama.2011.826

Kao, Y. H., Chen, Y. C., Lin, Y. K., Shiu, R. J., Chao, T. F., Chen, S. A., ... Chen, Y. J. (2014). FGF-23 dysregulates calcium homeostasis and electrophysiological properties in HL-1 atrial cells. *European Journal of Clinical Investigation*, *44*, 795–801. https://doi.org/10.1111/eci.12296

Kuro-o, M. (2011a). Klotho and the aging process. *The Korean Journal of Internal Medicine*, *26*, 113–122. https://doi.org/10.3904/kjim.2011.26.2.113

Kuro-O, M. (2011b). Phosphate and Klotho. *Kidney International*, *121*, S20–S23. https://doi.org/10.1038/ki.2011.26

Kuro-o, M., Matsumura, Y., Aizawa, H., Kawaguchi, H., Suga, T., Utsugi, T., ... Nabeshima, Y. I. (1997). Mutation of the mouse klotho gene leads to a syndrome resembling ageing. *Nature*, *390*, 45–51. https://doi.org/10.1038/36285

Lilley, E., Stanford, S. C., Kendall, D. E., Alexander, S. P. H., Cirino, G., Docherty, J. R., ... Ahluwalia, A. (2020). ARRIVE 2.0 and the British Journal of Pharmacology: Updated guidance for 2020. *British Journal of Pharmacology*. https://bpspubs.onlinelibrary.wiley.com/doi/full/10.1111/bph.15178

Lim, K., Lu, T. S., Molostvov, G., Lee, C., Lam, F. T., Zehnder, D., ... Hsiao, L. L. (2012). Vascular Klotho deficiency potentiates the development of human artery calcification and mediates resistance to fibroblast growth factor 23. *Circulation*, *125*, 2243–2255. https://doi.org/10.1161/CIRCULATIONAHA.111.053405

Memmos, E., Sarafidis, P., Pateinakis, P., Tsiantoulas, A., Faitatzidou, D., Giamalis, P., ... Papagianni, A. (2019). Soluble Klotho is associated with mortality and cardiovascular events in hemodialysis. *BMC Nephrology*, *20*, 217. https://doi.org/10.1186/s12882-019-1391-1

Nattel, S., Maguy, A., Le Bouter, S., & Yeh, Y. H. (2007). Arrhythmogenic ion-channel remodeling in the heart: Heart failure, myocardial infarction, and atrial fibrillation. *Physiological Reviews*, *87*, 425–456. https://doi.org/10.1152/physrev.00014.2006

Navarro-García, J. A., Delgado, C., Fernández-Velasco, M., Val-Blasco, A., Rodríguez-Sánchez, E., Aceves-Ripoll, J., ... Ruiz-Hurtado, G. (2019). Fibroblast growth factor-23 promotes rhythm alterations and contractile dysfunction in adult ventricular cardiomyocytes. *Nephrology, Dialysis, Transplantation*, *34*(11), 1864–1875. https://doi.org/10.1093/ndt/gfy392

Nowak, A., Friedrich, B., Artunc, F., Serra, A. L., Breidthardt, T., Twerenbold, R., ... Mueller, C. (2014). Prognostic value and link to atrial fibrillation of soluble Klotho and FGF23 in hemodialysis patients. *PLoS ONE*, *9*(7), e100688. https://doi.org/10.1371/journal.pone.0100688

Parks, R. J., Ray, G., Bienvenu, L. A., Rose, R. A., & Howlett, S. E. (2014). Sex differences in SR Ca(2+) release in murine ventricular myocytes

are regulated by the cAMP/PKA pathway. *Journal of Molecular and Cellular Cardiology*, *75*, 162–173. https://doi.org/10.1016/j.yjmcc.2014.07.006

Pavik, I., Jaeger, P., Ebner, L., Wagner, C. A., Petzold, K., Spichtig, D., ... Serra, A. L. (2013). Secreted Klotho and FGF23 in chronic kidney disease stage 1 to 5: A sequence suggested from a cross-sectional study. *Nephrology, Dialysis, Transplantation*, *28*, 352–359. https://doi.org/10.1093/ndt/gfs460

Percie du Sert, N., Hurst, V., Ahluwalia, A., Alam, S., Avey, M. T., Baker, M., ... Würbel, H. (2020). The ARRIVE guidelines 2.0: updated guidelines for reporting animal research. *PLoS Biol*, *18*, e3000410. https://doi.org/10.1371/journal.pbio.3000410

Pereira, L., Ruiz-Hurtado, G., Rueda, A., Mercadier, J. J., Benitah, J. P., & Gómez, A. M. (2014). Calcium signaling in diabetic cardiomyocytes. *Cell Calcium*, *56*, 372–380. https://doi.org/10.1016/j.ceca.2014.08.004

Ruiz-Hurtado, G., Li, L., Fernández-Velasco, M., Rueda, A., Lefebvre, F., Wang, Y., ... Gómez, A. M. (2015). Reconciling depressed Ca$^{2+}$ sparks occurrence with enhanced RyR2 activity in failing mice cardiomyocytes. *The Journal of General Physiology*, *146*, 295–306. https://doi.org/10.1085/jgp.201511366

Seiler, S., Wen, M., Roth, H. J., Fehrenz, M., Flügge, F., Herath, E., ... Heine, G. H. (2013). Plasma Klotho is not related to kidney function and does not predict adverse outcome in patients with chronic kidney disease. *Kidney International*, *83*, 121–128. https://doi.org/10.1038/ki.2012.288

Semba, R. D., Cappola, A. R., Sun, K., Bandinelli, S., Dalal, M., Crasto, C., ... Ferrucci, L. (2011). Plasma klotho and cardiovascular disease in adults. *Journal of the American Geriatrics Society*, *59*, 1596–1601. https://doi.org/10.1111/j.1532-5415.2011.03558.x

Shalhoub, V., Shatzen, E. M., Ward, S. C., Davis, J., Stevens, J., Bi, V., ... Richards, W. G. (2012). FGF23 neutralization improves chronic kidney disease-associated hyperparathyroidism yet increases mortality. *The Journal of Clinical Investigation*, *122*, 2543–2553. https://doi.org/10.1172/JCI61405

Shioya, T. (2007). A simple technique for isolating healthy heart cells from mouse models. *The Journal of Physiological Sciences*, *57*, 327–335. https://doi.org/10.2170/physiolsci.RP010107

Touchberry, C. D., Green, T. M., Tchikrizov, V., Mannix, J. E., Mao, T. F., Carney, B. W., ... Wacker, M. J. (2013). FGF23 is a novel regulator of intracellular calcium and cardiac contractility in addition to cardiac hypertrophy. *American Journal of Physiology. Endocrinology and Metabolism*, *304*, E863–E873. https://doi.org/10.1152/ajpendo.00596.2012

Urakawa, I., Yamazaki, Y., Shimada, T., Iijima, K., Hasegawa, H., Okawa, K., ... Yamashita, T. (2006). Klotho converts canonical FGF receptor into a specific receptor for FGF23. *Nature*, *444*, 770–774. https://doi.org/10.1038/nature05315

Verde, E., Pérez de Prado, A., López-Gómez, J. M., Quiroga, B., Goicoechea, M., García-Prieto, A., ... Luño, J. (2016). Asymptomatic intradialytic supraventricular arrhythmias and adverse outcomes in patients on hemodialysis. *Clinical Journal of the American Society of Nephrology*, *11*, 2210–2217. https://doi.org/10.2215/CJN.04310416

Wanner, C., Amann, K., & Shoji, T. (2016). The heart and vascular system in dialysis. *Lancet*, *388*, 276–284. https://doi.org/10.1016/S0140-6736(16)30508-6

Xiao, B., Jiang, M. T., Zhao, M., Yang, D., Sutherland, C., Lai, F. A., ... Chen, S. R. W. (2005). Characterization of a novel PKA phosphorylation site, serine-2030, reveals no PKA hyperphosphorylation of the cardiac ryanodine receptor in canine heart failure. *Circulation Research*, *96*, 847–855. https://doi.org/10.1161/01.RES.0000163276.26083.e8

Xie, J., Cha, S. K., An, S. W., Kuro-O, M., Birnbaumer, L., & Huang, C. L. (2012). Cardioprotection by Klotho through downregulation of TRPC6 channels in the mouse heart. *Nature Communications*, *3*, 1238. https://doi.org/10.1038/ncomms2240

Xie, J., Yoon, J., An, S. W., Kuro-o, M., & Huang, C. L. (2015). Soluble Klotho protects against uremic cardiomyopathy independently of fibroblast growth factor 23 and phosphate. *Journal of the American Society of Nephrology*, *26*, 1150–1160. https://doi.org/10.1681/ASN.2014040325

Yoshida, T., Fujimori, T., & Nabeshima, Y. (2002). Mediation of unusually high concentrations of 1,25-dihydroxyvitamin D in homozygous klotho mutant mice by increased expression of renal 1alpha-hydroxylase gene. *Endocrinology*, *143*, 683–689. https://doi.org/10.1210/endo.143.2.8657

## SUPPORTING INFORMATION

Additional supporting information may be found online in the Supporting Information section at the end of this article.

**How to cite this article:** Navarro-García JA, Rueda A, Romero-García T, et al. Enhanced Klotho availability protects against cardiac dysfunction induced by uraemic cardiomyopathy by regulating Ca$^{2+}$ handling. *Br J Pharmacol*. 2020;177: 4701–4719. https://doi.org/10.1111/bph.15235